TU TECHNISCHE
UNIVERSITÄT
WIEN WIEN

ATOMINSTITUT

DIPLOMARBEIT

Validation of MedAustron's Shielding Concept for Primaries Z ≤ 10

zur Erlangung des akademischen Grades

Diplom-Ingenieur

im Rahmen des Studiums

Biomedical Engineering

eingereicht von

Michael Bauer
Matrikelnummer 01555320

ausgeführt am Atominstitut
der Fakultät für Physik der Technischen Universität Wien
in Zusammenarbeit mit MedAustron

Betreuung
Univ.-Prof. Dr. Franz Josef Maringer,
Dr. Lukas Jägerhofer und
DI Claudia Lenauer

Wien, 15.10.2020

_____   _____
(Unterschrift Verfasser/in)   (Unterschrift Betreuer/in)

Danksagung

Ich möchte mich bei Lukas Jägerhofer für die ausgezeichnete Betreuung bedanken. Nicht nur mit seiner fachlichen Hilfe, sondern auch mit seinem Einsatz für mich bei MedAustron und CERN ist er mir über die Arbeit hinaus ein guter Mentor gewesen und hat mir den Weg zu einer neuen Herausforderung geebnet.

Ebenso möchte ich Claudia Lenauer, Michi Deutsch und Leo Schorn für die schöne Zeit während der Arbeits- und Pausenzeiten bei MedAustron danken. Insbesondere gilt mein Dank Claudia, die mir bei der Datenauswertung eine große Hilfe war, für meine Fragen stets bereit stand und regelmäßig wertvolles Feedback für mich parat hatte. Sowie Michi, der mich in FLUKA und weiteren IT Angelegenheiten geschult und mir außerdem bei den Arbeitswegen eine Mitfahrgelegenheit geboten hat.

Weiteres möchte ich meinem Betreuer seitens der TU Wien Univ.Prof. Dr. Franz Josef Maringer danken; der die Betreuung sehr spontan und unkompliziert übernommen hat. An dieser Stelle möchte ich auch das von ihm organisierte Adventsymposium des ÖVS hervorheben, wodurch der Kontakt zu Lukas und somit die Masterarbeit überhaupt zustande gekommen ist.

Ich möchte mich weiteres bei EBG MedAustron für die Möglichkeit bedanken, diese Arbeit in Form eines Praktikums absolviert haben zu dürfen und die damit verbundene finanzielle Unterstützung und Bereitstellung von Equipment.

Darüber hinaus gilt mein Dank Dr. Albert Hirtl, der sein Büro mit mir geteilt und mir zusätzliche Rechenleistung verschafft hat.

Ich möchte auch meinen Eltern danken, durch deren Unterstützung ich mich während meiner gesamten Studienzeit ganz auf meine Ausbildung fokussieren habe können.

Abschließend möchte ich Laura danken. Während all der Zeit hat sie mich bestmöglich motiviert und unterstützt.

Erklärung

Ich erkläre eidesstattlich, dass die vorliegende Arbeit von mir selbstständig und nach den anerkannten Grundsätzen wissenschaftlichen Arbeitens verfasst wurde. Es wurden ausschließlich jene Quellen und Hilfsmittel, insbesondere jene Literatur, verwendet, die als solche kenntlich gemacht wurden.

Abstract

Radiation therapy is a state of the art method to treat cancer and is performed with photons and electrons, but also much heavier particles, namely ions. At MedAustron but also at most other facilities worldwide ion therapy is currently accomplished using protons and carbon ions. The reason for the use of various particles is the difference in each biological effect. Regarding the assumption that there is no perfect ion for all kind of tumors, the ability to choose from various projectiles is beneficial for individual treatments[16]. Therefore, it is more and more investigated in the use of additional ions in cancer therapy.

This work is the foundation for the authorization of ion beams beyond protons and carbon ions at MedAustron. It is based on and compared to Jägerhofer[1], Feldbaumer[2] and Karacson[3]. It validates the shielding concept for primary particles $Z \leq 10$ using Monte Carlo simulations. In addition to ambient dose equivalent calculations outside two shielded irradiation rooms, air activation on the inside is considered.

Beyond that, a model is introduced that takes the energy, the mass- and charge number of the primary particle as input and computes the ambient dose equivalent H*(10) outside of an arbitrary shielding. Using the results of a few simulations of different ions in a certain geometry, the values for further ions in the corresponding geometry can be conservatively predicted. Thereby a considerable amount of Monte Carlo simulations and associated computational cost is economized.

Kurzfassung

Strahlentherapie ist Teil der modernen Krebsbehandlung und fungiert mit Photonen und Elektronen, aber auch mit schwereren Teilchen, nämlich Ionen. MedAustron und andere Einrichtungen weltweit verwenden für die Ionentherapie hauptsächlich Protonen und Kohlenstoffionen. Der Grund, warum verschiedene Teilchen eingesetzt werden, ist der Unterschied der jeweiligen biologischen Effekte. Es wird vermutet, dass es kein einzelnes Ion gibt, das die gesamte Tumortherapie bestmöglich abdeckt. Die Option von unterschiedlichen Projektilen zu wählen, bietet somit einen erheblichen Vorteil im Hinblick auf individuelle Behandlungen[16], wodurch auf eine Erweiterung der therapeutisch eingesetzten Primärteilchen gesetzt wird.

Diese Arbeit dient MedAustron als strahlenschutztechnische Grundlage für die Verwendung von Projektilen bis $Z \leq 10$ und basiert auf den bereits bewilligten und umgesetzten Szenarien der Arbeiten von Jägerhofer[1], Feldbaumer[2] und Karacson[3]. Zum einen wird die Umgebungs-Äquivalentdosis außerhalb der Abschirmungen zweier Bestrahlungsräume betrachtet und zum anderen die verursachte Luftaktivierung innerhalb der Räume.

Darüber hinaus wird ein Modell vorgestellt, das anhand der Energie, Massen- und Ladungszahl eines Primärteilchens, die davon verursachte Umgebungs-Äquivalentdosis H*(10) außerhalb einer beliebigen Abschirmung konservativ abschätzt. Anhand der Ergebnisse einzelner Simulationen unterschiedlicher Ionen in einer bestimmten Geometrie können die Werte für weitere Ionen in der entsprechenden Geometrie konservativ vorhergesagt werden. Damit kann eine große Zahl von Monte Carlo Simulationen und damit verbundener Rechenaufwand eingespart werden.

4

Contents

Contents

6

List of Abbreviations

MC Monte Carlo

RBE Relative Biological Effectiveness

LET Linear Energy Transfer

OER Oxygen Enhancement Ratio

PER Peak to Entrance Ratio

OAR Organs At Risk

HIMAC Heavy Ion Medical Accelerator in Chiba

GSI Gesellschaft für Schwerionenforschung

HIT Heidelberger Ionenstrahl-Therapiezentrum

CNAO Fondazione Centro Nazionale Adroterapia Oncologica

IR1 Irradiation Room 1

IR3 Irradiation Room 3

p800 primary, proton with 800 MeV

c400 primary, carbon ion with 400 MeV/u

a time unit, year*

*On behalf of practicality the time unit "year" was used. It is not part of the international system of units and was defined as $1\ a = 31\ 556\ 926\ s$ according to [32].

1 Introduction

1.1 A Short History of Hadron Therapy

In 1930 Ernest Lawrence invented the cyclotron in Berkeley. Two years later in 1932 Sir James Chadwick discovered the neutron, and shortly after, Ernest and his brother John Lawrence experimented with fast neutrons on biological systems. In 1938 the first patients were treated in Berkeley, using neutrons, produced by the reaction of 8 MeV deuterons impinging on a Beryllium target.[1] Thereby 250 patients were treated by John Lawrence and and R.S. Stone.[5] In 1946 Robert Rathbun 'Bob' Wilson, a former student of Lawrence and later founder of the Fermi-lab, proposed already 1946 the use of proton beams in radiation oncology.[6] Additionally he predicted the relevance of heavier nuclei, such as very energetic carbon atoms in future cancer treatment.[1] 1948 extensive studies by Berkeley confirmed Wilson's prediction and 1954 the first patients were treated using protons in Berkeley.[5] In 1957 in Uppsala the first patient in Europe was treated using proton beams. Soon afterwards the Harvard Cyclotron Facility adapted their cyclotron for the treatment of patients. In the following years proton therapy centres opened in Dubna, Moscow and St. Petersburg. The first treatment with helium ions was performed in 1957 and the use of neon ions followed 1975. At that point, however, none of the treatment methods made use of the fact that ions and protons carry a charge and are therefore easy to detect and steer. Therefore, it was necessary to use collimators and compensators for the beam shapping (see Chapter 1.4).

In 1994 a facility for the treatment with carbon beams was built in Chiba (Japan) named Heavy Ion Medical Accelerator in Chiba (HIMAC). Based on a successful pilot project in Darmstadt (GSI), 2001 the Heidelberg Ion Therapy Centre (HIT) was approved and the building process started 2003. In 2005 the manufacturing of Fondazione Centro Nazionale Adroterapia Oncologica (CNAO) started in Pavia and two years later the construction of MedAustron in Wiener Neustadt, both facilities featuring proton and carbon therapy.[7]

1.2 Medical Advantages of Ion Therapy

The therapeutic usage of hadrons, such as protons and carbon ions enables a decisive reduction of radiation exposure of healthy tissue compared to methods using electrons and photons as illustrated in figure 1.1. When a fast, charged particle moves through matter, it ionizes atoms and deposits a dose. Thereby energy of its charged particles decreases, while the interaction cross section increases, which leads to the formation of

8

a peak in terms of energy depostion at the end of its path, called Bragg peak. Energy lost by charged particles E_p is inversely proportional to the square of their velocity v_p,

$$E \propto v_p^{-2}$$

which explains the peak occurring just before the particle comes to a complete stop. [8]
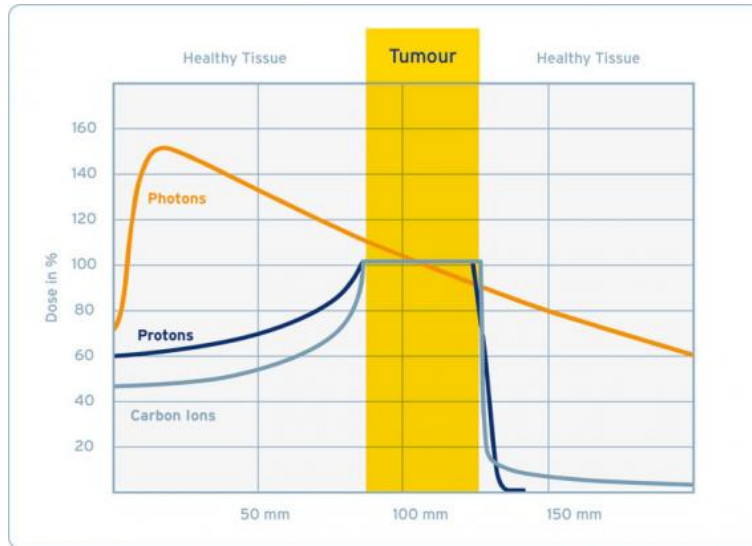
Figure 1.1: Depth dose distribution for treatment of protons (blue), carbon ions (grey) and photons (orange) assuming a 40 mm wide tumore in 85 to 125 mm tissue depth. In this graph the beam is coming from the left side. It illustrates the reduction of radiation exposure of healthy tissue in front and especially behind the tumor by hadron compared to photon and electron therapy. [4]

By combining various beam energies, the peak can be adjusted according to individual treatments. Due to the low exposure of healthy tissue, higher doses can be used and tumors resistant against conventional radiotherapy become treatable. [3]

1.3 MedAustron

MedAustron possesses one irradiation room (IR) for non clinical research (IR1) and three for clinical usage (IR2-IR4), including one with a horizontal beam outlet, one with a horizontal and vertical beam outlet and one with a proton gantry. An overview of the complex can be seen in figure 1.2.

The proton and carbon ions are provided by three ion sources, where CO_2 or H_2 is heated to extremely high temperatures, resulting in plasma. The ions are then extracted by the use of electric fields. Next, they are accelerated by the linear accelerator to $7MeV/u$ (12% of the speed of light) and then passed to the synchrotron. At a circumference
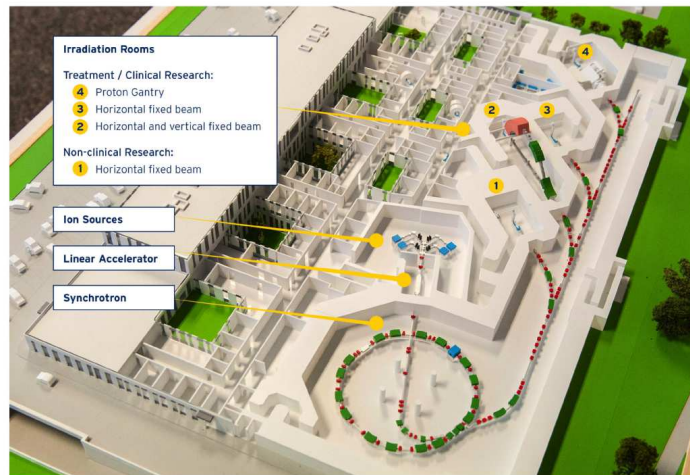
Figure 1.2: Model of the MedAustron facility, including the ion sources, the linear accelerator, the synchrotron and the irradiation rooms.[4]

of 80 m they are accelerated up to 2/3 of the speed of light and finally guided to the irradiation rooms. Protons used for tumor therapy have energies between $60 - 250 MeV$ and carbon ions between $120 - 400 MeV/u$. In IR1 protons up to 800 MeV are authorized for research. The intensity of the beam has its maximum for protons at $2E10$ and for carbon ions at $1E09$ particles per spill. A single spill is sufficient for scanning about one cross section of the tumor.

1.4 Motivation for Ions in Hadron Therapy Beyond Protons and Carbon Ions

After Wilson[6] proposed the use of protons beside neutrons, the interest in different ions, such as helium, carbon, neon and argon for therapy has been ongoing due to their potential biological advantages and improved dose localization. Therefore, a lot of historical data is available, however, it needs to be considered that in the past they used a different beam delivery system. Historically, all therapy centres used a passive scattering technique, as against today, where most of the modern facilities, like HIMAC, HIT, CNAO and MedAustron apply an active scanning technique.[10] According to the **passive scattering technique** the beam is spread by placing a scattering material into the path of the incoming particles. A combination of collimators and compensators delivers the dose to the target volume. To spread out the Bragg Peak, a set of range modulator wheels or ridge filters are added into the beam line. This technique is usually used with cyclotrons. The concept is shown in figure 1.3 (top). In the **active scanning technique**, magnets deflect and steer the particle beam. Guided by the control system, the

scanning magnet steer the single mono-energetic beam to paint voxel by voxel the target volume, in successive layers. The penetration depth of the Bragg peak is adjusted by varying the initial kinetic energy of the beam. This technique is used with synchrotrons and reaches a precision of $0.5mm$. The concept is shown in figure 1.3 (bottom).[11]
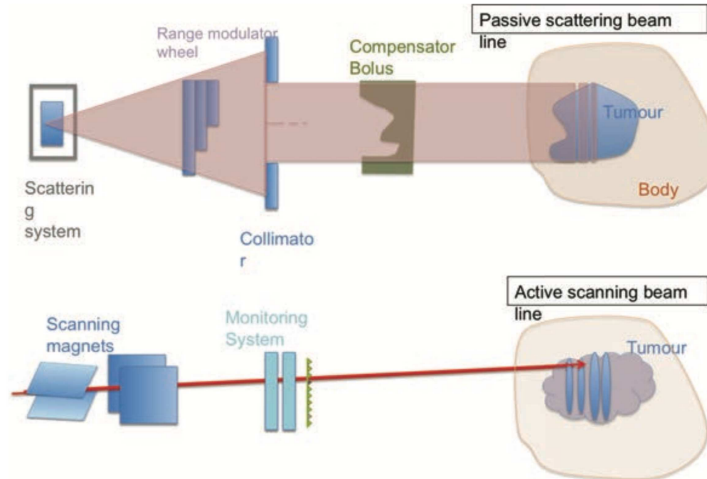

Figure 1.3: Passive scattering and active scattering beam delivery systems[11]

In general different beam delivery systems imply differences in dose rate, Linear Energy Transfer (LET) and dose distribution. Therefore, historical data need to be used with caution.[12] For many diseases it does not influence the quality of the treatment. For tumors influenced by organ movement, e.g. lung cancer, however, one must be aware of potential interplay between the motion of the target and the delivery of the radiation field.[10]

In this chapter ions with $Z \leq 10$ are discussed, which are of interest in future radiotherapy. According to Knäusl et. al.[16] it is not assumed that there is the perfect ion for the whole field of radiotherapy, but the ability to choose from various ions might be beneficial for individual treatments.

1.4.1 Helium

There have been ongoing studies regarding the use of helium ions in radiotherapy, some of them are introduced in this chapter.

In 1974, Anas M. El-Mahdi et. al.[13] published a pre-clinical animal experience comparing the isoeffective dose caused by Co-60 and He-4. They focused on lung tumors in mice and found that He-4 was more effective for occult as well as manifest tumors, due to a higher LET. However, they could not finally answer, whether the treatment with He-4 is more effective, because of missing information about the Relative Biological

Effectiveness (RBE).

In 1986, John T. Lyman et. al.[14] published his research on stereotactic radiosurgery in the central nervous system using helium ions, retrieved from a $184inch$ synchrotron. Showing an improved dose localization and dose distribution for the radiosurgery of neurological patients with intracranial arteriovenous malformations (abnormal connections between the arteries and veins in the brain).

More recent studies are the one by Grün[15] and Knäusl[16].

To compare helium ions with protons and Carbon ions, Grün et. al.[15] analysed the Peak to Entrance Ratio (PER) of the physical dose (PER_{PHYS}), the RBE (PER_{RBE}) and the RBE-weighted dose (PER_{BIO}) for different dose levels, field configurations and tissue types. Grün found that helium combines the good PER_{BIO} of Carbon ions with the better PER_{PHYS} of protons. In addition to a sharper Bragg peak, helium ions cause a reduced lateral penumbra (reduced range straggling and scattering), i.e. they show an improved dose localization compared to protons. Thus, they are expected to represent an effective, intermediate alternative to protons and Carbon ions overcoming each of their weaknesses.

Knäusl et. al.[16] created treatment plans for various patients with helium ions and protons using the same software. The plans for helium ions were slightly better compared to protons in terms of Organs At Risk (OAR) sparing for selected patients and tumor geometries. Especially for young Neuroblastoma (third most common malign tumor of children) patients the dose in the liver, the kidney and the total body volume could be reduced significantly. Figure 1.4 visualizes that most of the surrounding tissue and the OAR received less dose using helium instead of protons. Similar reductions were found for Ependymoma (represents 10 % of all brain tumors in children) patients.
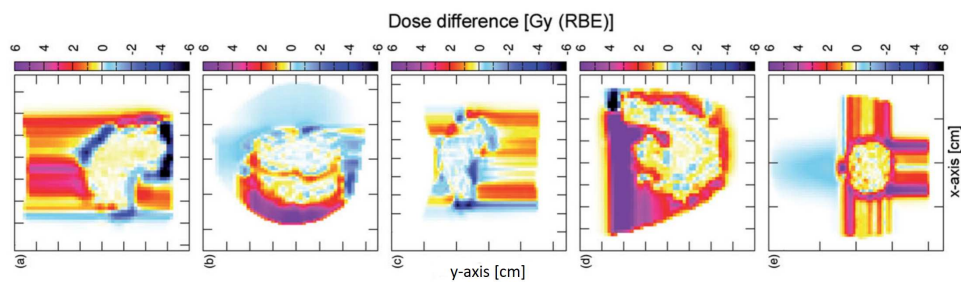

Figure 1.4: The red shaded areas represent voxels receiving more dose in the proton plans, while the blue shaded areas represent those voxels receiving more dose in the helium ion plans. Various tumors are shown: (a) Neuroblastoma, (b) Wilms tumor, (c) Hodgkin lymphoma, (d) Ewing sarcoma, (e) Ependymoma[16]

In 2021, HIT is planning to start the first clinical programme using helium ions in therapy. MedAustron plans to implement helium ions as well.

1.4.2 Oxygen

To overcome the radiation resistance of hypoxic tumors, O-16 ions have become part of particles evaluated for radiotherapy in the recent years. Due to their high Z, O-16 ions have a large LET and therefore a high RBE. On the one hand that leads to more biological damage in the tumor region, but on the other hand it also leads to more damage of healthy tissue. Therefore Sokol et al.[17] suggest to use them in combined beams with lighter ions. Another advantage of O-16 ions is the high survival of cells in the entrance channel, shown in figure 1.5. An increase in entrance cell survival of up to 13% compared to C-12 ions could be calculated using TRiP98 by Sokol[17]. For further steps towards O-16 ions in therapy pre-clinical and clinical tests are necessary.
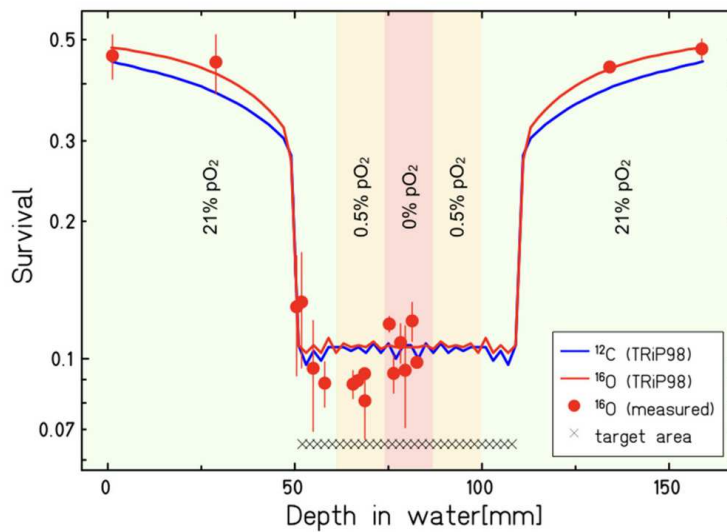

Figure 1.5: Survival distribution for a two-field plan comparing C-12 and O-16. The error bars represent the standard error of two of the corresponding independent experiments. The shaded colors of the areas correspond to the differently oxygenated regions.[17]

2 Physical Background

2.1 Radiobiological Basics

In the following a few terms are defined and discussed, that are essential to understand the impact of radiation on biological systems. The Relative Biological Effectiveness **RBE** is one of them and describes the ratio of the absorbed dose of a reference radiation D_{ref} (usually $250keV$ X-rays or Co-60 gamma rays) to the absorbed dose from a test radiation D_x causing the same biological effect, e.g. cell survival.[9]

$$RBE := \frac{D_{ref}}{D_x} \tag{2.1}$$

The RBE increases with the Linear Energy Transfer **LET** shown in figure 2.1, which is defined as

$$LET := \frac{dE}{dx}. \tag{2.2}$$

In the same figure it can be observed that the radiation with x-rays results in a lower RBE than the one with hadrons. The higher Z, the higher the RBE in general. The heavier a particle, the less it is slowed down in a tissue, but once it is slowed down, it releases all the energy in a small vicinity, which leads to a high LET and a dense ionization. In contrast, lighter particles like photons release their energy in a bigger range and therefore have a low LET and a thin ionization.

Figure 2.2 shows the LET on the x- and the RBE on the y-axis. The higher the ionization density, the more irreversible double strand breaks are caused on the DNA. As soon as the the energy needed to inactivate a cell is exceeded, the efficiency decreases due to an overkill. RBE_{max} is reached around a $LET \approx 100kev/\mu m$.

Another essential quantity is the **Oxygen Enhancement Ratio (OER)**, which describes the influence of oxygen on biological effects. It is defined as the ratio of hypoxic to aerobic doses needed to achieve the same biological effects.

$$OER = \frac{O_{hypoxic}}{O_{aerobic}}. \tag{2.3}$$

14
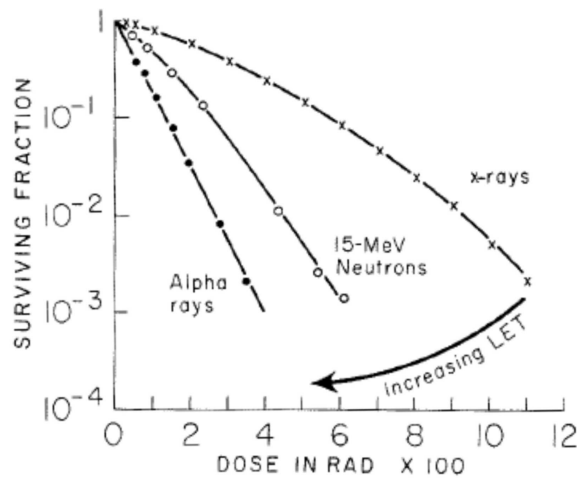
Figure 2.1: Dose in Rad on the x- and the cell surviving fraction on the y-axis. Increasing LET for different particles. [9]
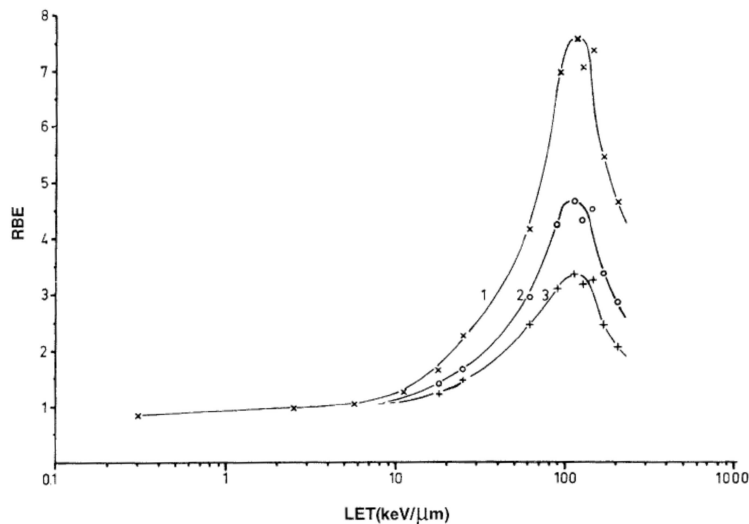
Figure 2.2: The LET on the x- and the RBE in $keV/\nu m$ on the y-axis. The labels 1,2,3 refer to different levels of survival (0.8, 0.1, 0.01). The RBE reaches a maximum around $100keV/\mu m$. [9]

In general the value for OER is between $2-4$. Hence, cells with sufficient oxygen supply are more sensitive to radiation. Hypoxic cells activate an energy saving mode, whereby less cell divisions take place and since this is the phase where cells are most vulnerable, radiation causes less harm. The effect is shown in figure 2.3

The higher the LET, the less important is the effect of the oxygen effect as shown in figure 2.4.
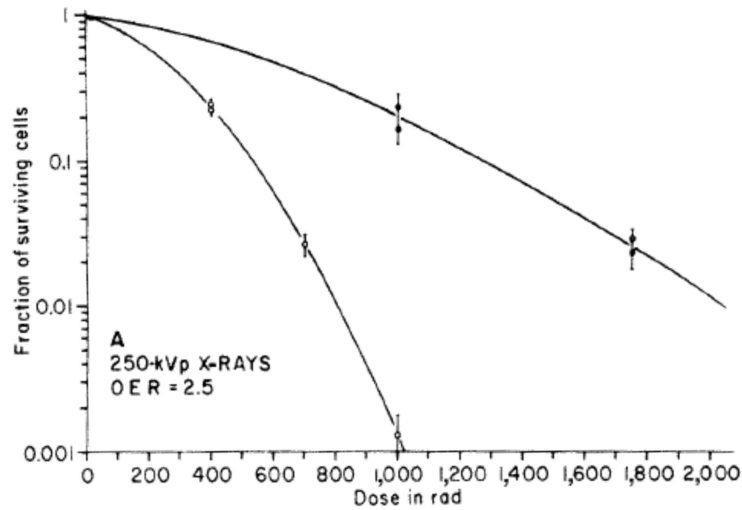
Figure 2.3: This graph shows the effect of the Oxygen supply in biological systems with and without sufficient oxygen supply. The filled circles show an aerobic system, the empty circles show a hypoxic one.[9]
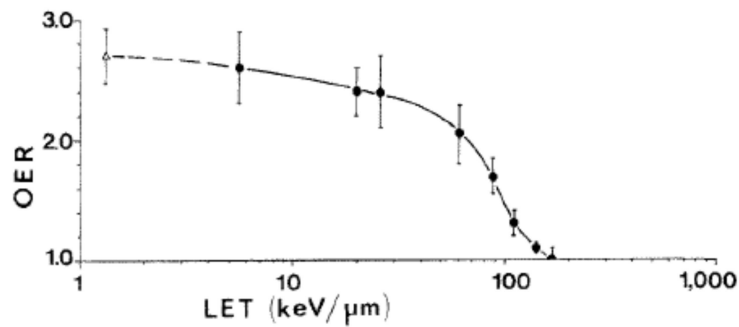
Figure 2.4: With increasing LET, the OER decreases.[9]

2.2 Dosimetric Basics

In the following essential quantities in the field of radiation protection are introduced.

2.2.1 Physical Quantities

- Fluence Φ
  With the number of particles dN incident on a sphere of cross sectional area da the fluence is defined as

$$\Phi = \frac{dN}{da} \tag{2.4}$$

16

with the unit m^{-2}.[19] In dosimetric calculations, as in FLUKA, it is expressed in terms of particle trajectory length:

$$\Phi = \frac{dl}{dV}. \tag{2.5}$$

- Absorbed Dose D
  It is the measure for the mean energy $\bar{E}$ imparted to matter with mass dm

$$D = \frac{\bar{E}}{dm} \tag{2.6}$$

with the unit $Jkg^{-1} \equiv Gray$.[19]

- Cross Section σ
  It is the measure of a target for a particular interaction caused by incident particles. With the probability P of an interaction for a single particle when subjected to a particle fluence Φ:

$$\sigma = \frac{P}{\Phi} \tag{2.7}$$

with the unit m^2.[19]

2.2.2 Operational Quantities

- Ambient Dose Equivalent $H^*(d)$
 At a certain point in a radiation field it is the dose equivalent that would be produced by the corresponding expanded field in the ICRU sphere at a depth d opposing of the aligned field. Recommendations are $d = 10mm$ for penetrating radiation as it is used in this work.

  The ICRU sphere is a tissue equivalent sphere with a defined diameter of $30cm$ and a composition by mass of 76.2% Oxygen, 10.1% Hydrogen, 11.1% Carbon and 2.6% Nitrogen. The total density is $1g/cm^3$.[18]

- Directional Dose Equivalent $H^*(d, \Omega)$
  Analogue to $H^*(d)$, but in addition the angle of incidence Ω is considered.[18]

2.2.3 Protection Quantities

- Organ Equivalent Dose H_T
  The equivalent dose H_T in a tissue T, irradiated in a radiation field consisting of several radiations with different values of w_R is given by

$$H_T = \sum_R w_R D_{T,R} \tag{2.8}$$

with the unit *Sievert*. Where $D_{T,R}$ is the average absorbed dose from a specific radiation type R in tissue T.[18] Values for w_R are specified in table 2.1.

Radiation	w_R
Photons	1
Electrons and Muons	1
Protons and Pions	2
α particles and Heavy Ions	20
Neutrons: $E_n < 1 MeV$	$2.5 + 18.2e^{-[ln(E_n)]^2/6}$
Neutrons: $1 MeV leq E_n \leq 50 MeV$	$5.0 + 17.0e^{-[ln(2E_n)]^2/6}$
Neutrons: $E_n > 50 MeV$	$2.5 + 3.25e^{-[ln(0.04E_n)]^2/6}$

Table 2.1: Values for radiation weighting factors recommended by ICRP. [19]

Tissue or Organ	w_T	$\sum w_T$
Gonads	0.08	0.08
Red bone marrow, Colon, Lung, Stomach, Breasts, Remainder Tissue*	0.12	0.72
Bladder, Liver, Oesophagus, Thyroid	0.04	0.16
Bone Surface, Brain, Salivary glands, Skin	0.01	0.04

Table 2.2: Tissue weighting factors recommended by ICRP. [19] *Remainder Tissue: Adrenals, Extra thoracic region, Gall bladder, Heart, Kidneys, Lymphatic nodes, Muscle, Oral mucosa, Pancreas, Prostate, Small intestine, Spleen, Thymus, Uterus/cervix.

- Effective Dose H_E
  The effective dose is defined by

$$H_E = \sum_T w_T H_T \qquad (2.9)$$

with the unit *Sievert*. Where T represents a tissue in the human body, H_T is the dose equivalent in the tissue T and w_T is a weighting factor reflecting the sensitivity of the tissue towards irradiation as specified in table 2.2.

2.3 Interactions of Neutrons with Matter

In this chapter various neutron interactions with matter are described. Concerning the type of interaction, the energy of the neutron is of major importance. A common classification is listed in table 2.3.

2.3.1 Microscopic Approach

If a large number of monoenergectic neutrons impinge on a target, some of them interact and change their energy and or direction. Some pass through the target and others may

Neutron Classification	Energy Range
Cold	$< 0.01 eV$
Thermal	$0.01 eV$ - $0.3 eV$
Epithermal	$0.3 eV$ - $10 keV$
Fast	$10 keV$ - $20 MeV$
Relativistic	$> 20 MeV$

Table 2.3: Classification of neutrons by their energy[20]

be absorbed and vanish. Each possible interaction occurs with a certain probability. This probability divided by the number of target atoms per unit area is called cross section σ and has the dimension of an area m^2. Besides the energy of the incident neutron the interaction depends on the mass of the nucleus. The interactions can be divided as shown in figure 2.5.
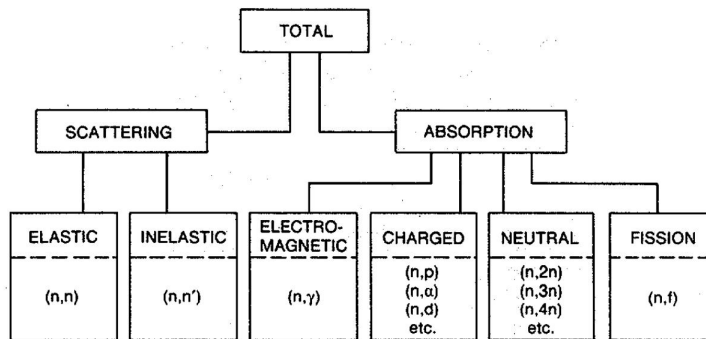
Figure 2.5: Types of neutron interactions with matter.[21]

In general the interactions are divided into scattering and absorption. During elastic scattering the neutron transfers kinetic energy to the nucleus (in contrast to photon scattering). The neutron changes its direction and its energy decreases, depending on the weight of the nucleus as follows

$$\frac{E_{before}}{E_{after}} = \frac{2E_{before}A}{(A+1)^2} \tag{2.10}$$

with the atomic weight A of the nucleus. Due to the similar mass, hydrogen is the most effective material for moderation. During the collision with a hydrogen atom, the neutron loses half of its energy on average. In contrast to elastic scattering, inelastic scattering excites the nucleus. Therefore, the nucleus not only gains kinetic energy, but also emits high energetic gamma radiation. When the neutron is absorbed by the target nucleus various particles can be emitted or fission can be induced.[21]

2.3.2 Macroscopic Approach

The microscopic approach can be used to understand interactions of a neutron with a single nucleus, calculations become too complicated, however, for thick targets made up from various elements. Therefore, the macroscopic cross section can be used. Whereby the target can be considered as a series of atomic layers and thus for each layer the results from the microscopic cross section approach can be applied. By integration over enough atomic layers to reach the depth x in the target sample, the intensity of the neutron beam is given as

$$I(x) = I_0 e^{-N\sigma_t x} \tag{2.11}$$

with the intensity of the incident beam I_0, the atom density N and the microscopic cross section σ_t, which depends on the neutron energy. So the intensity of a neutron beam in matter decreases exponentially. The total macroscopic cross section is defined as

$$\Sigma_t = N\sigma_t \tag{2.12}$$

with the unit cm^{-1}. Based on the macroscopic cross section the mean-free-path length λ is defined as

$$\lambda = \frac{1}{\Sigma_t}. \tag{2.13}$$

Using λ neutron detectors and neutron shielding can be evaluated. If the mean-free-path length is small compared to the size of a detector volume, the detection efficiency is high and if the thickness of a shielding is many times the mean-free-path length, it is sufficient.

3 Materials and Methods

Monte Carlo (MC) Simulations play an important role in modern particle and radiation physics. They give an insight into physical concepts and furthermore, enable predictions about quantities of complex systems. Decisive for the application of MC simulations is the progress in computer performance. In the field of particle transport, modern computers enable the calculation of the movement of a huge number of particles, so called cascades, in complex geometries in a reasonable amount of time. Beyond that more and more comprehensive MC software packages have been developed. In this work the software package FLUKA[22;23;24] ("FLUktuierende KAskade") is used.

3.1 FLUKA

FLUKA was originally designed for evaluation of NaI crystals used as hadron calorimeters. It developed from a code specialising in high energy accelerator shielding to a general purpose MC code for simulation of particle transport through matter. It enables the transport of about 60 different particles like hadrons, heavy ions and electromagnetic particles with a "microscopic" approach where each step has a sound physical basis.

3.1.1 Materials

A set of 25 common materials and compounds is provided by FLUKA, for instance air. In addition it is possible to define arbitrary materials. In this work, MedAustron concrete and heavy concrete are defined specifically and apart from that all used materials are predefined, like air, iron and tungsten. The materials are assigned to the geometry elements called Regions (described in Chapter 3.1.2). There is one special component worth mentioning, the so called "BLCKHOLE", that absorbs all incident particles. It surrounds the entire geometry, so that the movement of the particles stops eventually, where it is no longer of interest. In this work BLCKHOLE is also used to focus CPU power. (additional to Biasing, described in chapter 3.1.3). Whilst, the beam is stopped by BLCKHOLE material in directions without interest for a particular simulation. In table 3.1 the compositions of concrete (density = 2.4 g/cm^3), heavy concrete (density = 4.2 g/cm^3) and air (density = 0.00120484 g/cm^3) are listed.

	Concrete (mass-%)	Heavy Concrete (mass-%)	Air (mass-%)
Hydrogen	0.47	0.28	
Nitrogen			75.5267
Oxygen	49.28	32.13	23.1781
Aluminium	0.4	0.25	
Silicon	1.47	0.69	
Sodium		0.02	
Calcium	35.8	2.1	
Potassium	0.09	0.06	
Argon		0.16	1.2827
Carbon	10.4	0.01	0.01248
Magnesium	1.68	0.21	
Iron	0.09	63.96	
Titanium	0.05	0.03	
Sulphur	0.27	0.16	

Table 3.1: Chemical composition of the compounds used for the simulations, given in percentage of total mass.

3.1.2 Geometry

In combinatorial geometry more complex Regions are built from fundamental Bodies like cylinders, cubes and planes with Boolean operations like unions, differences and intersections. The three dimensional visualization tool SimpleGeo[25] simplifies the building process. SimpleGeo provides an export format readable by FLUKA as well as a powerful debugging tool. In this work generic cylindrically symmetrical geometries are built to represent the original building plan (figure 3.1). Figure 3.2 corresponds to the lateral site of Irradiation Room 1 (IR1) with heavy padding and figure 3.3 represents the lateral site ofIrradiation Room 3 (IR3) with normal concrete and a thicker target.

Inside the cylindrical geometry a beam is shot along the positive z-axis against a lead target. We want to score different quantities (see chapter 3.1.4) outside of the cylindrical shielding, namely laterally and frontally. To achieve a higher computing efficiency this is done using two different geometries that vary in terms of BLCKHOLE material used (Chapter 3.1.1) and Biasing (Chapter 3.1.3).

3.1.3 Biasing

Biasing methods are an important tool to save CPU time during shielding calculations in complex geometries. The use of biasing methods replaces the actual physical problem with a mathematically similar one to obtain the same solutions with faster statistical convergence. In this work "Importance Biasing" is used, which works fine for thick shielding geometries. For the biasing the shielding blocks need to be segmented as can

Figure 3.1: The original geometry of the irradiation room 1,2 and 3 of MedAustron compared to the generic cylindrically symmetrical geometry of IR1 and IR3 for lateral scoring. [1]
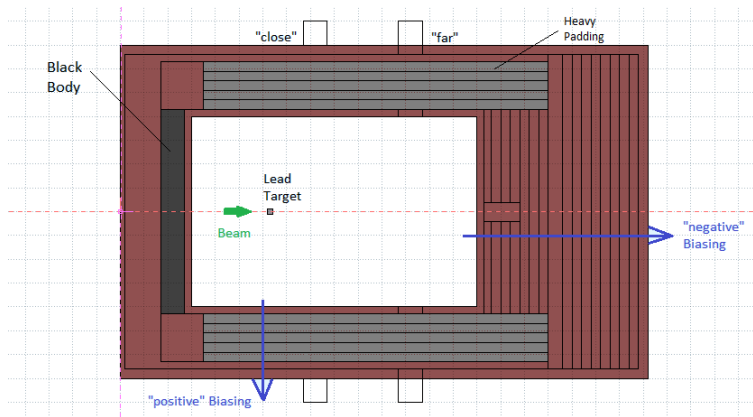

Figure 3.2: Cylindrically symmetrical geometry for the lateral site of irradiation room 1. Apart from normal concrete heavy padding is used.

be seen in figure 3.2 and 3.3. Each segment is then assigned an importance factor between 10^{-4} and 10^4. These factors increase exponentially from the inside out according to

$$importance\ factor = startvalue * e^{number\ of\ sector} \qquad (3.1)$$

If particles enter from another region with a lower importance factor, the number of particles is multiplied with the ratio of the importance factors, while the weight of each particle, with which each one contributes to the result, is reduced by the ratio of the importance factors. This event is called "Splitting". If a particle, however, enters a region
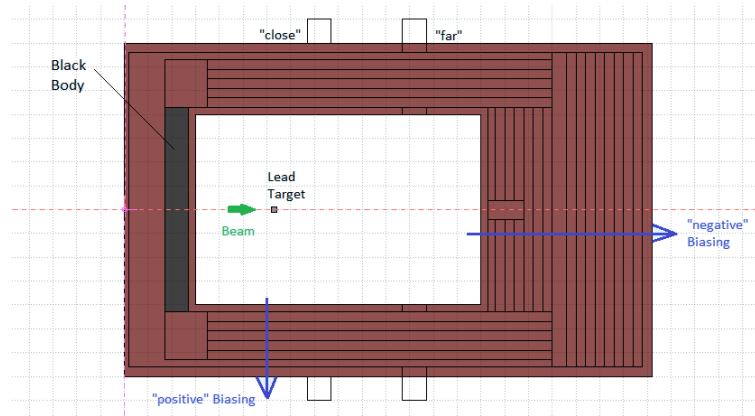
Figure 3.3: Cylindrically symmetrical geometry for the lateral site of irradiation room 3. In contrast to irradiation room 1 it does not contain any heavy padding.

coming from another region with a higher importance factor the number of particles is reduced by the ratio of the importance factors while the individual weights are increased by this ratio. This method is called "Russian Roulette". By the use of these methods the CPU power can be concentrated onto significant regions.[22]

3.1.4 Scoring

In Fluka there are various scoring methods available to obtain the desired results. Those used in this work are listed in the following.

- With USRBIN different quantities like the particle fluence, the ambient dose equivalent H*(10) and the absorbed dose can be scored in a predefined volume with an arbitrary spatial resolution that can be defined by a bin size. The results can be shown in a color plot where each color is related to a defined range of values.[22]

- With USRTRACK the track-length fluence inside a defined region can be scored. Different particle types can be chosen, as well as the energy range of the particles.[22]

As scoring volumes the detectors "close" and "far" are used for lateral and "front" for frontal scoring. They can be seen in figure 3.2 and 3.3.

3.2 Particle Transport

The particle transport in FLUKA is based on physical principles using the interaction probability, which is given for different materials by their cross sections. The particles differ in the probability to interact with the nuclei of a material and are therefore distinguished into hadrons (e.g. protons and neutrons) and leptons (e.g. electron and muon).

The building blocks for hadrons are quarks and experience strong interaction and therefore have a high tendency to interact with nuclei. If a high energetic hadron impinges on nucleus, further protons and neutrons are emitted from the nucleus, which have enough energy to cause further collisions. This phenomenon is called hadron cascade. In contrast to hadrons, lepton and photon interactions with nuclei are electromagnetic or with the electrons surrounding the nucleus, which can lead to high energetic electron and gamma secondary radiation. This phenomena is called electromagnetic cascade.[2]

3.2.1 Hadronic Interaction

In contrast to electromagnetic interaction, which is well understood and accurately described by quantum electrodynamics, we have no theory that describes inelastic hadronic interactions in a complete way. Since analytic approaches usually depend on a high number of approximations, numeric methods with MC approaches are preferred. The numeric calculation in FLUKA is ensured by the PEANUT model[26] (PreEquilibrium Approach to NUclear Thermalization) which can be separated in the Intra-Nuclear-Cascade-, Pre-Equilibrium- and Equilibrium phase, which find application depending on the energy. Overall FLUKA covers energies from 2.5 GeV down to 10 MeV for charged hadrons and 20 MeV for neutrons. The transport of neutrons with energies below 20 MeV is described at the end of the current chapter.

The **Intra-Nuclear-Cascade** model[27] [28] describes the nucleus according to the Fermi gas model, as an accumulation of fermions inside a potential well. If the nucleus is in its ground state, the lowest energy levels are occupied according to the Pauli exclusion principle and the energies of all nucleons are beneath the Fermi level.[29]. The incident hadron initiates a chain reaction of collisions by the nucleons in the nucleus. Thus, the energy of the nucleons is raised beyond the Fermi level. Due to the ongoing collisions of fermions the introduced energy finally spreads evenly on all nucleons in the nucleus. Eventually all nucleons reach energies below $100 MeV$ and the Intra-Nuclear-Cascade models become inaccurate. At that point **pre-equilibrium models** are used to describe the thermalization, where particles on high energy levels relax and more and more holes (excitons) emerge in the lower energy levels and act as mobile charge carriers. Meanwhile, more and more high energetic hadrons are emitted. The equilibrium is reached, if the number of excitons beneath the Fermi energy is nearly constant. Finally, in the **equilibrium phase** the excitation energy of the nucleus is released by evaporation (multiparticle emission) and nuclear fission.

Interactions of neutrons below energies of 20 MeV are processed in group transports, whereby they are separated in 260 energy groups. The corresponding cross sections are based on data received by measurements and are stored in a library, containing information about isotopic production for more than 250 different materials. In addition the interactions may cause photons, which are transported in groups as well.[24]

3.2.2 Electromagnetic Interaction

In FLUKA models for the photoelectric effect, the pair production, the Compton- and Rayleigh scattering are implemented. The model for Compton scattering even considers atomic bonds and orbital movements using data from libraries. Beyond that a model for the photonuclear reaction is offered, which is not part of the default settings and needs to be activated manually. [24]

The energy loss and the deflection of the charged particles caused by the electromagnetic interactions is not computed directly, but statistically approximated. A constant energy loss dE/dx on macroscopic step sizes between two interaction points is assumed, based on a corresponding stopping power. Consequently, changes in directions are only possible during the interaction points. If one assumes high particle deflection, e.g. in magnetic fields, the step size needs to appropriately set.

3.3 Activation of Air

The air in accelerator facilities, where beam losses occur is either ventilated and recycled or released into the environment. Due to interactions of hadronic and electromagnetic cascades the air may become activated. In pure air, that mainly consists of Oxygen, Nitrogen, Argon and CO_2 about 39 radionuclides with half live times longer than a few seconds are produced.

For the activation calculations a generic geometry is no longer useful, because the results depend on the volume of the room. Thus, the original rectangular geometry of IR1 is implemented and used; it is shown in figure 3.4.
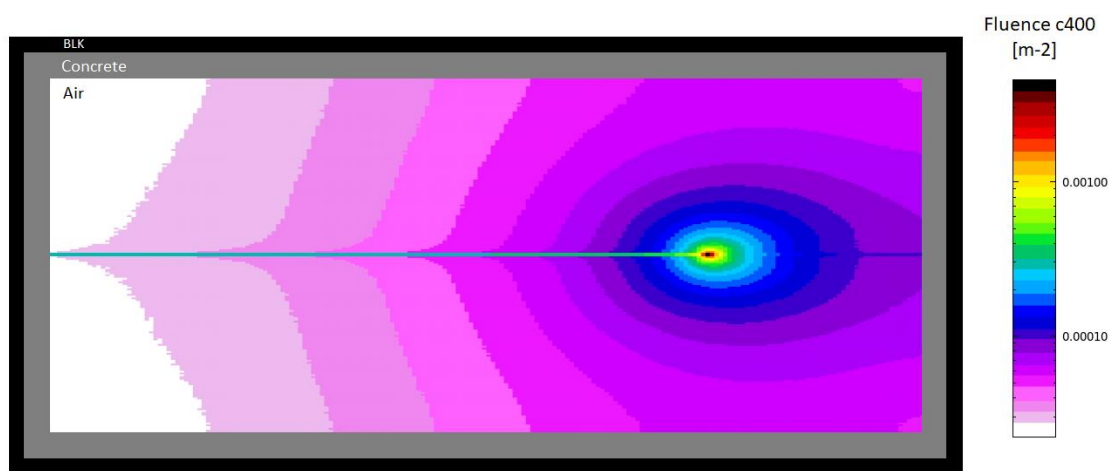

Figure 3.4: Front view of the original geometry of IR1. The color scale illustrates the result of the USRBIN for the total fluence caused by carbon primaries with $400 MeV/u$ (c400).

With RESNUCLEi residual nuclei produced in inelastic interactions can be scored. The results depend on internal models and libraries for elements and materials of FLUKA. To obtain reasonable results with RESNUCLEi two additional physics cards are activated, namely COALESCE and EVAPORAT for the generation and evaporation of of heavy fragments.[24]

The irradiation profile was chosen according to Karacson[3] with an irradiation time of $1161\,s$ and an intensity of $2E09\,primaries/s$. Considering that the maximum intensity of MedAustron's accelerator for protons with 800 MeV is $2E10\,primaries/s$ and the one for carbon ions with $400 MeV/u$ is $1E9\,primaries/s$ this is still conservative.

4 Results and Discussion

4.1 Annual Ambient Dose Equivalent Rate

The annual ambient dose equivalent maps of C-12 with 400 MeV/u for the IR1 and IR3 for the lateral site are shown in figure 4.1 and 4.2. In the same graphs the simulated values for the annual dose rate at detector "close" and "far" are given. The values are based on the authorized number of C-12 primaries per year, namely $7.8E14\ primaries/a$. The terminus dose refers to the ambient dose equivalent $H^*(10)$.
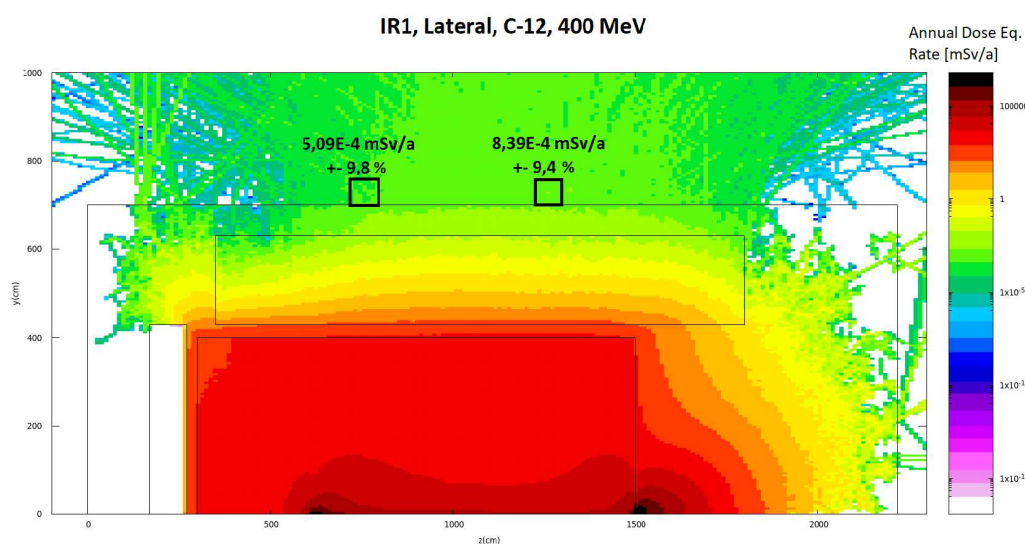

Figure 4.1: Lateral annual dose equivalent map of C-12 with 400 MeV in the IR1.

Due to the higher range in materials of protons with 800 MeV that are used already, compared to primaries with Z ≤ 10 with 400 MeV/u, simulations focusing on the frontal region of the IR1 are not necessary in terms radiation protection. The IR3 possesses a thicker target, whereby the primaries do not pass, as can be seen in the dose distribution of the room in figure 4.2. For that reason radiation protection focuses again on the lateral region only.

In table 4.1 the results of detector "far" are compared to the ones by Jägerhofer[1], who put a detector on a comparable location in the original geometry.

As can be observed in table 4.1, even though different FLUKA versions were used and
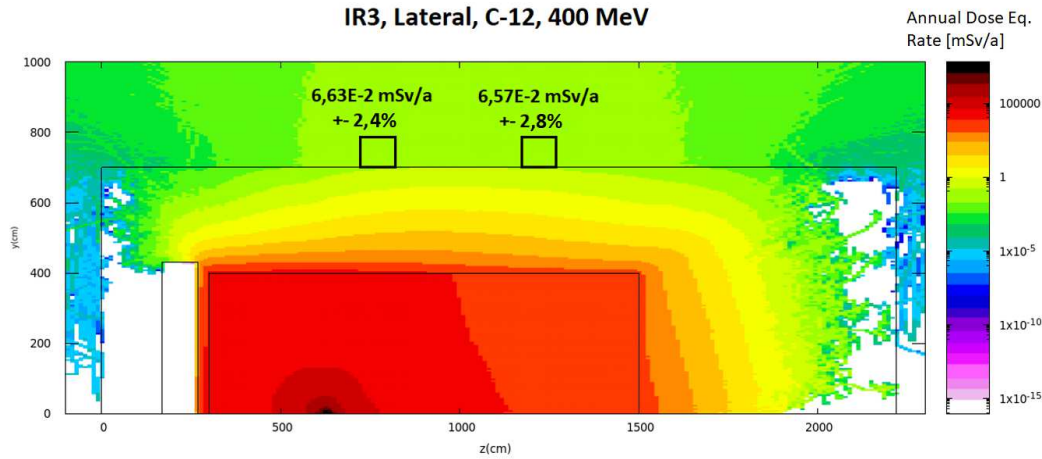
28

Figure 4.2: Lateral annual dose equivalent map of C-12 with 400 MeV/n in the IR3.

	detector "far"	Jägerhofer[1]
C-12, 400 MeV/u in IR1	$8.39E-04\ mSv/a\ \pm\ 9.4\%$	$2.15E-03\ mSv/a$
C-12 400 MeV/u in IR3	$6.57E-02\ mSv/a\ \pm\ 2.8\%$	$5.53E-02\ \pm\ 2.3\%$

Table 4.1: Comparison of the the annual ambient dose equivalent results in IR1 and IR3 from this work and the ones from Jägerhofer[1].

the detectors are not quite on the same location, the generic geometry achieves equivalent results. In the following the results for primaries beyond C-12 are introduced. Beforehand, however, an approximation for the neutron yield is introduced, which is important for the discussion of the ambient dose equivalent results.

4.1.1 Kurosawa Approximation for the Neutron Yield

According to Kurosawa et al.[30], the neutron yield Y of a target depends on the energy E_p and the proton number Z_p of the projectile, as well as the neutron N_p, N_t and mass number A_p, A_t of projectile and target and can be approximated as

$$Y = \frac{1.5 \cdot 10^{-6}}{N_t^{1/3}} E_p^2 \left(A_p^{1/3} + A_t^{13} \right)^2 N_p \frac{A_p}{Z_p^2}. \tag{4.1}$$

In figure 4.3 the yield is shown for different primaries and energies. In this work we focus on $E_p = 400\ MeV/u$, since this is the maximum energy for all $Z \leq 10$ using the MedAustron facility.
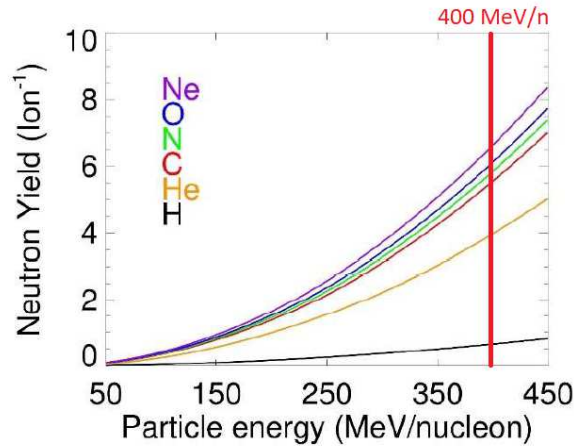
Figure 4.3: Kurosawa[30] approximation of the neutron yield (y-axis) with the energy of the projectile on the x-axis for different primaries. The red line illustrates the 400 MeV/u, which is the energy of interest in the following chapter.[31]

4.1.2 Approximation for the Annual Ambient Dose Equivalent Rate

In this chapter the results for the annual ambient dose equivalent values for all stable ions $Z \leq 10$ are introduced and discussed. The following values are based on the authorized amount of protons with $250 MeV$ in IR1, which is $7.8E15\ primaries/a$. This value serves as a rather conservative approximation. The actual number of primaries will not be discussed in detail here, but in any case lies substantially below the number given above. By sketching the annual dose equivalent of various particles together with the mass number, a characteristic behaviour can be observed. This behaviour shows a strong dependency on the ratio of protons to neutrons and is similar to the one of the neutron yield approximation by Kurosawa[30]. This correlation is illustrated in figure 4.4 for the detector "close" and "far" in IR3 using $E_p = 400\ MeV/n$.

It may thus be concluded that the proton to neutron ratio influences the dose in a similar way as the yield. In a further step we, therefore, alter the approximation of the neutron yield eq. 4.1 to obtain a model for the ambient dose equivalent rate.

$$\dot{H}^*(10, E_p, A_p) = \frac{\alpha}{N_t^{1/3}} E_p^2 \left(A_p^{1/3} + A_t^{13} \right)^2 N_p \frac{A_p}{Z_p^2} \tag{4.2}$$

with the parameter α of dimensions

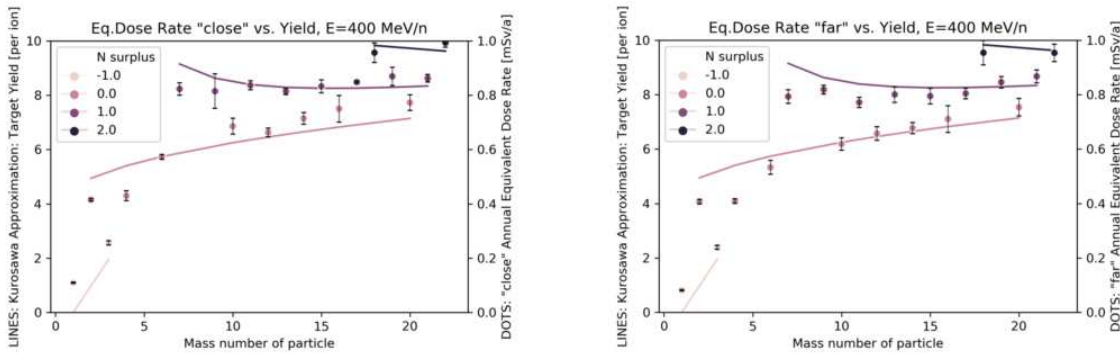$$[\alpha] = \frac{mSv}{a \cdot MeV^2}. \tag{4.3}$$

Figure 4.4: Annual ambient dose equivalent rate results of the detector "close" (left) and "far" (right) outside the shielding of IR3 compared to the neutron yield in the target region for 400 MeV/u. The mass number is represented by the x-axis. The simulated dose values for all stable ions $Z \leq 10$ are represented by the right y-axis and by DOTS. The calculated neutron yield values in the target region according to the approximation by Kurosawa[30] are represented by the left y-axis and by LINES. The color corresponds to the neutron surplus of the primary particles.

Equation 4.2 must not be interpreted as a fit, but rather as a conservatively estimated model. The approximation is visualized in figure 4.5. For both of the detectors the same, conservative value

$$\alpha = 3.75E - 09 \ \frac{mSv}{a \cdot MeV^2}$$

is chosen.

Next it is looked at the ambient dose equivalent results of the two detectors in IR1, and again they are viewed together with the Kurosawa approximation of the neutron yield in figure 4.6.

This time, however, it is obvious that the two quantities no longer correlate. The proton to neutron ratio no longer influences the ambient dose equivalent. Beside the heavy concrete, the only difference in the simulations of the IR1 is the bombarded target. As described in chapter 3.1.2 the length of the target for the IR1 is only 0.5 cm compared to 20 cm in IR3. Therefore, the Bragg peak is easily captured in the thicker IR3 target, while it is outside the thin target of the IR1 (figure 4.7). Due to this far lower number of interactions between the beam and the target, the proton to neutron ratio of the projectile is no longer essential for the results and the model is not applicable. In this scenario the dose equivalent rate increases linearly with the mass number of primaries, as shown in figure 4.8.
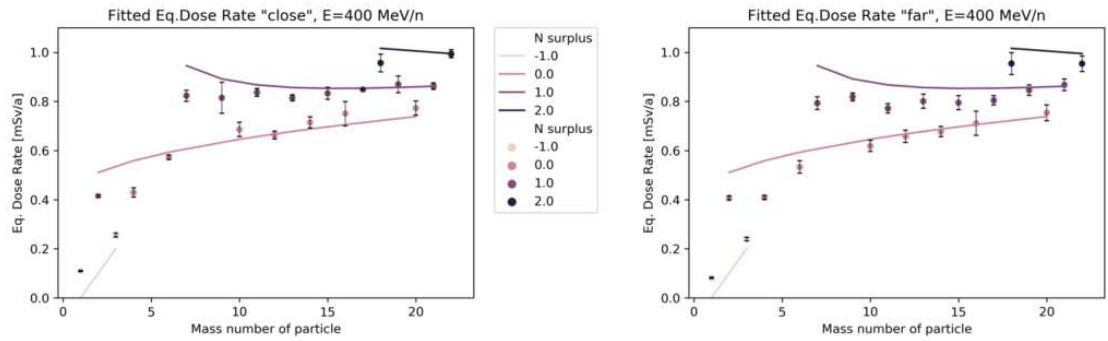
Figure 4.5: A model of the annual ambient dose equivalent rate outside the shielding based on the Kurosawa[30] approximation of the neutron Yield. The simulated dose rate values of detector "close" (left) and "far" (right) for all stable ions $Z \leq 10$ are represented by DOTS. The predicted values of the model are represented by LINES and calculated with the parameter $\alpha = 3.75E - 09 \frac{mSv}{a \cdot MeV^2}$. The color corresponds to the neutron surplus of the primary particles.
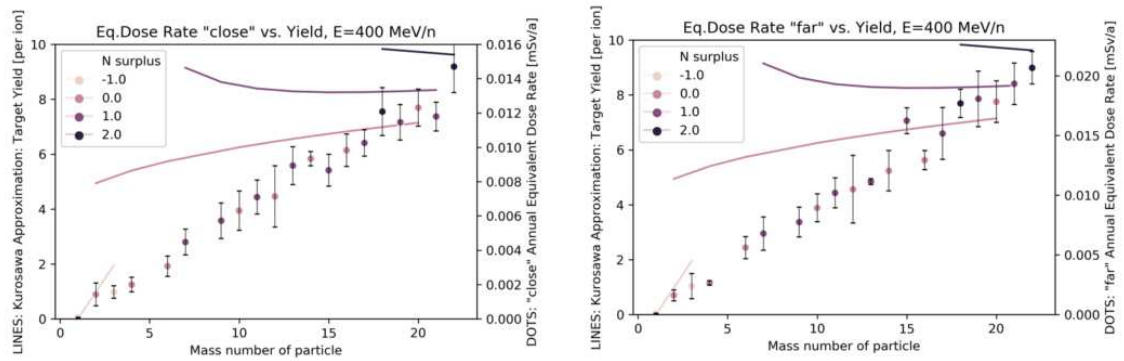
Figure 4.6: Annual ambient dose equivalent rate results of the detector "close" (left) and "far" (right) outside the shielding of IR1 compared to the neutron yield in the target region for 400 MeV/u. The mass number is represented by the x-axis. The simulated dose values for all stable ions $Z \leq 10$ are represented by the right y-axis and by DOTS. The calculated neutron yield values in the target region according to the approximation by Kurosawa[30] are represented by the left y-axis and by LINES. The color corresponds to the neutron surplus of the primary particles.
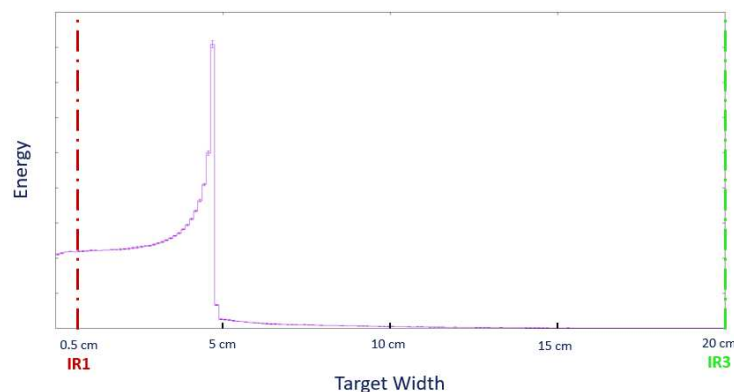
Figure 4.7: This graph illustrates the capturing of the Bragg peak with the IR3 target (green) and shows that it is outside the IR1 target (red). The shown peak is caused by C-12 with $400MeV/u$.
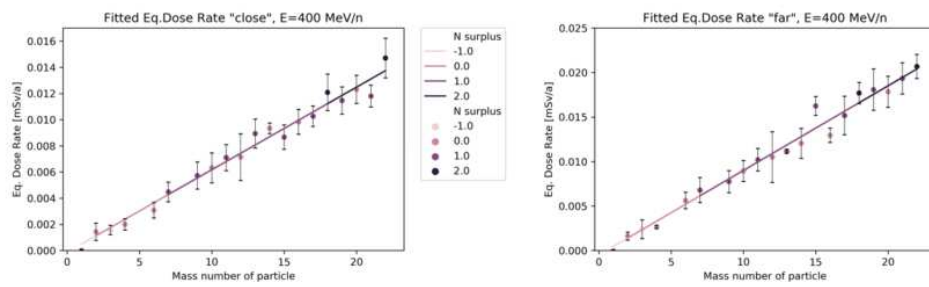
Figure 4.8: Linear fit of the dose equivalent rate values of the two detectors. For both of the them the correlation coefficient $r = 0.99$. The standard uncertainty $\sigma_{close} = 2.28E - 05mSv/a$ for the detector "close" and $\sigma_{close} = 3.43E - 05mSv/a$ for "far".

4.2 Activation of Air

In this section the activity results of air activation are shown and discussed. Radionuclides caused by activation together with the magnitude of their absolute activities in IR1 are shown in figure 4.9. The bright green colour represents high activity values, while the dark blue one represents low activity values. All nuclides up to neon with $400 MeV/u$ and protons with $800 MeV$ are shown. In the latter case the results from this work (p800), but also the ones from Karacson[3] ($p800_{Karacson}$) are portrayed. From all the activation products five are outstanding, namely O-15, N-13, C-11, O-14 and Ar-41. It is noticeable that the activities from these five radionuclides are quite similar for all of the primary particles, including the authorized protons.
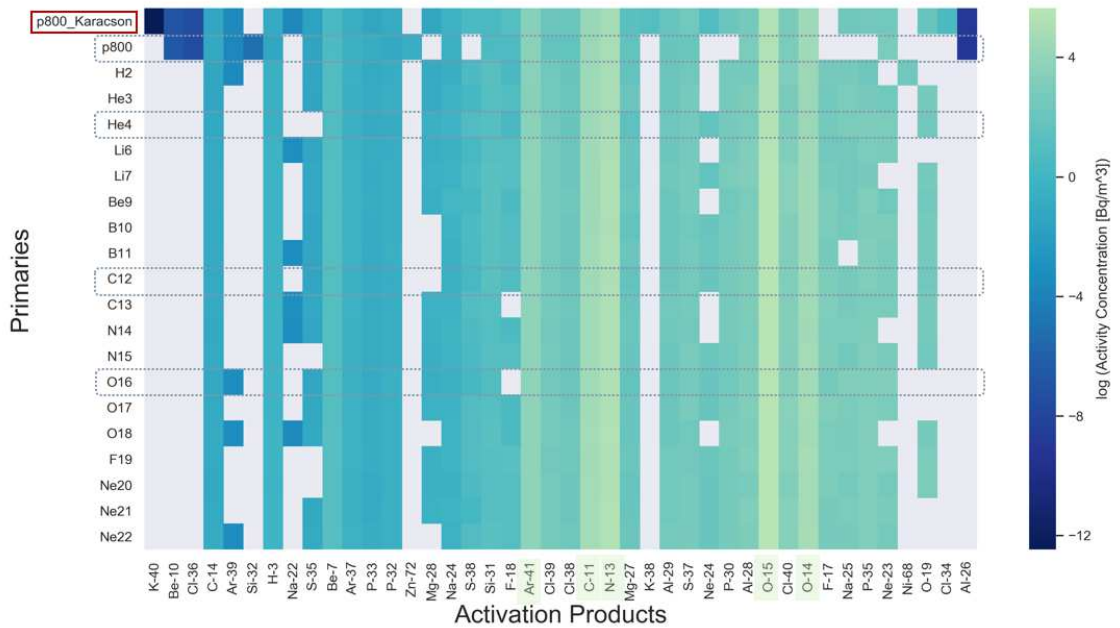
Figure 4.9: Magnitude of activities of activation products of primaries H-2 to Ne-22 with $400\ MeV/u$ compared to Karcson's[3] protons with $800\ MeV$ (p800).

The values are further compared in the bar chart in figure 4.10, where the activities of the four heaviest ions of interest are plotted relative to the activities of authorized protons with 800 MeV[3]. The red line in the graph indicates where the ratio of activities is one. It can be observed that most of the values are below those of p800, however, the different intensities need to be kept in mind. They are $2E09\ primaries/s$ for the ions with $400 MeV/u$ and $2E10\ primaries/s$ for the protons with $800 MeV$, as described in section 3.3. Ne-24 is the only activation product for which some of the "heavy" ions show higher activity values than for the authorized protons. From all the simulated ions, F-19 causes the highest activity of this β_- emitting activation product with a value of $168 Bq/m^2 \pm 50\%$. First, this activity is rather small considering the fact that is is inside

a monitored area. Second, the half life time of Ne-24 is only 3.38 *min* and third, the uncertainty of the value is rather big. Therefore, the fact that some of the "heavy" ions cause higher activity values than protons seems to be innocuous.

Figure 4.10 only compares the results of the four heaviest ions to the authorized p800. In the appendix in section 6.3 the same comparison is shown for all the other primaries $Z \leq 10$. In the same section of the appendix, bar charts of the absolute activities can be found.

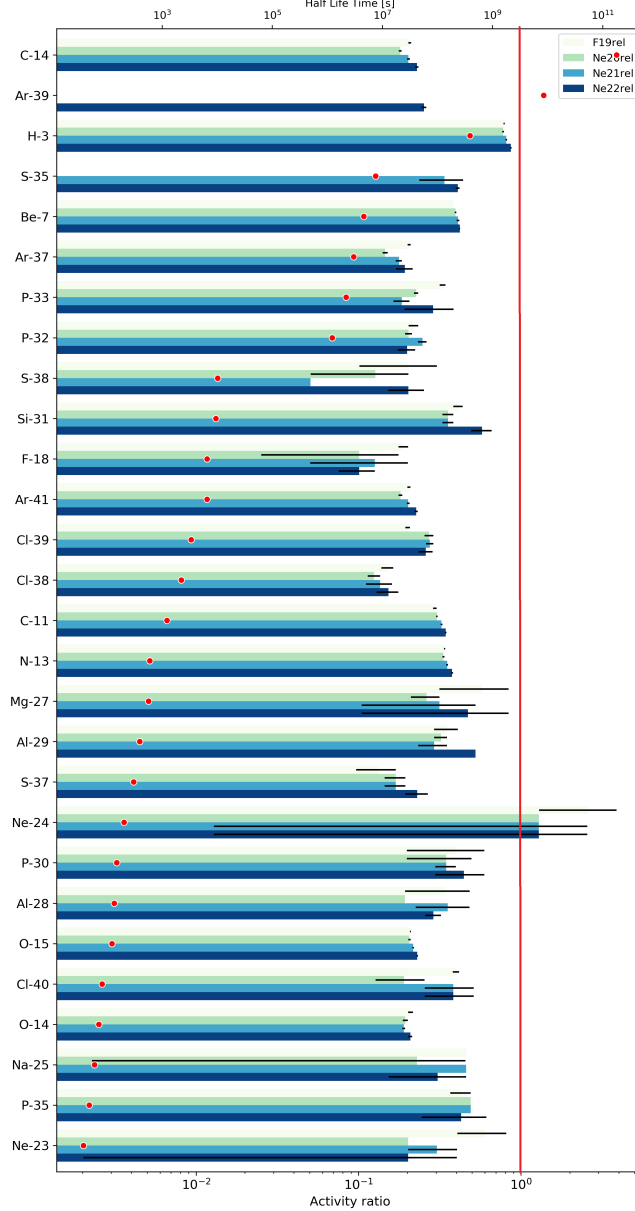Figure 4.10: Activation products from primaries F-19 to Ne-22 (in various colors) are shown on the y-axis. The ratio of the activity concentrations to the authorized p800 from the work of Karacson[3] is shown on the bottom x-axis. The values are sorted by the nuclide half life time, which is also plotted on the top x-axis together with red points. The red line indicates where the ratio of activities is one.

5 Conclusions and Outlook

The shielding concept of two representative irradiation rooms of MedAustron was verified for all stable ions up to $Z \leq 10$. Using the Monte Carlo simulation package FLUKA, the ambient dose equivalent $H^*(10)$ outside the shielding was calculated in a generic, cylinder-symmetric geometry. Beyond that, air activation inside one of the rooms was computed. Since this calculation highly depends on the volume of air, a realistic geometry was designed for that purpose. For both, the ambient dose equivalent and the activation calculations, the results are consistent with the outcome of previous papers by Jägerhofer[1], Feldbaumer[2] and Karacson[3].

Even though, the ambient dose equivalent outside the shielding on the lateral side increases by the use of heavier ions than C-12, the values don't change significantly and stay below an annual ambient dose equivalent rate of $1\ mSv/a$. This is still very conservative, considering that the concerned area is monitored and justifies values up to $6\ mSv/a$. Regarding air activation, it was shown that ions up to neon with 400 MeV/u cause a similar activation like protons with 800 MeV, which are already authorized. Therefore, it can be concluded that the shielding is sufficient for the use of primaries up to neon.

Further, it was found that the proton to neutron ratio influences the dose in a characteristic way, similar as the neutron yield does. Based on an approximation of the neutron yield in the target region by Kurosawa[30], a model for the ambient dose equivalent outside an arbitrary shielding was introduced. The model requires that the Bragg peak of the primary particle needs to be inside the targets volume, otherwise there is hardly an interaction between the beam and the target. The model takes the energy, the mass- and charge number of the primary particle as input. Using the results of a few simulations for different ions in a certain geometry, the values for further ions in the corresponding geometry can be conservatively predicted. Thereby a considerable amount of Monte Carlo simulations and associated computational costs can be economized.

One of the next steps towards the authorization of new particles is the calculation of the inhalation dose caused by air activation, which was not part of this work anymore. Besides air, it also needs to be considered that materials of the irradiation rooms can be activated. Potentially activated materials are copper, steel (Inox 316LN), magnetic steel (Isovac 250-35 A and Isovac 1300-100 A), aluminium, electronic scrap, concrete and heavy concrete.

5 Conclusions and Outlook

Further, it is worked on a concept that compares different particles for the relevance of radiation protection and on a budget for the use of various primaries.

This work validated the shielding concept for all stable primaries up to neon, due to the analogy of the various calculations. In practice, however, it is going to take decades, just to realize the implementation of a few of them. The clinically most relevant ones appear to be helium and oxygen. Helium ions are planned to be the next particles accelerated at MedAustron. First it is going to be used in preclinical research and eventually for the treatment of patients.

38

6 Appendix

6.1 FLUKA Files

In this section FLUKA files are introduced that were generated for this work. Two different input files are listed, one for the ambient dose equivalent and another for the activation calculations. The output of the ambient dose equivalent simulations are scored with the USRBIN card and can be seen in chapter 4. The simulation for the activation of air generates "sum.lis" files, in which the activation products together with their corresponding activity are given. The data was then processed by the use of python.

6.1.1 Input File: Ambient Dose Equivalent

Input file of the ambient dose equivalent simulations for the primary Ne-20.

```
TITLE
Ne20
GLOBAL          1000.0        0.0          0.0          0.0          1.0          0.
DEFAULTS                                                                       PRECISIO
GEOBEGIN                                                                       COMBNAME
0    0          MC-CAD
* a
XYP a           270.00
* a1
RCC a1          0.00 0.00 1530.00 0.00 0.00 30.00 430.00
* a2
RCC a2          0.00 0.00 1560.00 0.00 0.00 40.00 430.00
* a3
RCC a3          0.00 0.00 1600.00 0.00 0.00 40.00 430.00
* a4
RCC a4          0.00 0.00 1640.00 0.00 0.00 40.00 430.00
* a5
RCC a5          0.00 0.00 1680.00 0.00 0.00 40.00 430.00
* a6
RCC a6          0.00 0.00 1720.00 0.00 0.00 40.00 430.00
* a7
RCC a7          0.00 0.00 1760.00 0.00 0.00 40.00 430.00
* ain
```

```
RCC ain        0.00 0.00 170.00 0.00 0.00 180.00 430.00
* aou
RCC aou        0.00 0.00 170.00 0.00 0.00 180.00 630.00
* b1
RCC b1         0.00 0.00 350.00 0.00 0.00 1450.00 430.00
* b2
RCC b2         0.00 0.00 350.00 0.00 0.00 1450.00 470.00
* b3
RCC b3         0.00 0.00 350.00 0.00 0.00 1450.00 510.00
* b4
RCC b4         0.00 0.00 350.00 0.00 0.00 1450.00 550.00
* b5
RCC b5         0.00 0.00 350.00 0.00 0.00 1450.00 590.00
* b6
RCC b6         0.00 0.00 350.00 0.00 0.00 1450.00 630.00
* bb
RCC bb         0.00 0.00 1530.00 0.00 0.00 270.00 430.00
* blk
SPH blk        0.00 0.00 0.00 100000.00
* c
RCC c          0.00 0.00 1800.00 0.00 0.00 380.00 660.00
* c1
RCC c1         0.00 0.00 1800.00 0.00 0.00 60.00 660.00
* c2
RCC c2         0.00 0.00 1860.00 0.00 0.00 40.00 660.00
* c3
RCC c3         0.00 0.00 1900.00 0.00 0.00 40.00 660.00
* c4
RCC c4         0.00 0.00 1940.00 0.00 0.00 40.00 660.00
* c5
RCC c5         0.00 0.00 1980.00 0.00 0.00 40.00 660.00
* c6
RCC c6         0.00 0.00 2020.00 0.00 0.00 40.00 660.00
* c7
RCC c7         0.00 0.00 2060.00 0.00 0.00 40.00 660.00
* c8
RCC c8         0.00 0.00 2100.00 0.00 0.00 40.00 660.00
* c9
RCC c9         0.00 0.00 2140.00 0.00 0.00 40.00 660.00
* co
RCC co         0.00 0.00 20.00 0.00 0.00 2160.00 660.00
* conou
RCC conou      0.00 0.00 0.00 0.00 0.00 2220.00 700.00
* flu1
```

```
RCC flu1        0.00 0.00 1170.00 0.00 0.00 100.00 430.00
* flu11
RCC flu11       0.00 0.00 1170.00 0.00 0.00 100.00 400.00
* flu3
RCC flu3        0.00 0.00 1170.00 0.00 0.00 100.00 700.00
* flu33
RCC flu33       0.00 0.00 1170.00 0.00 0.00 100.00 660.00
* flu4
RCC flu4        0.00 0.00 1170.00 0.00 0.00 100.00 800.00
* flu5
RCC flu5        0.00 0.00 770.00 0.00 0.00 100.00 700.00
* flu5
RCC flu6        0.00 0.00 770.00 0.00 0.00 100.00 800.00
* fu
RCC fu          0.00 0.00 170.00 0.00 0.00 1630.00 630.00
* gul
RCC gul         0.00 0.00 170.00 0.00 0.00 1630.00 430.00
* iron
RCC iron        0.00 0.00 1530.00 0.00 0.00 100.00 40.00
* rin
RCC rin         0.00 0.00 300.00 0.00 0.00 1200.00 400.00
* targ
RCC targ        0.00 0.00 620.00 0.00 0.00 20. 10.
* void
RCC void        0.00 0.00 -500.00 0.00 0.00 3230.00 1500.00
* voidB0
PLA voidB0      1.00000 0.00000 0.00000 1.000 0.000 -500.000
END
* Reg # 1
* BLK; assigned material: Blackhole; mat # (1)
BLK         5 +blk  -( +void  +voidB0 ) -( +void  -voidB0 )
* Reg # 2
* VOID; assigned material: Oxygen; mat # (8)
VOID        5 +void  -conou  -( +flu4  -flu3) -( +flu6 - flu5)
* Reg # 3
* CON; assigned material: Aluminium; mat # (10)
CON         5 +conou  -co  -( +flu3  -flu33 )
* Reg # 4
* FUL; assigned material: Gold; mat # (15)
FUL         5 +co  -fu  -c
* Reg # 5
* TV3; assigned material: Gold; mat # (15)
TV3         5 +gul  +a
* Reg # 6
```

6 Appendix

```
* H; assigned material: Argon; mat # (20)
H          5 +fu  -( +b2  -b1 )  -( +b3  -b2 )  -( +b4
-b3 )  -( +b5  -b4 )  -( +b6  -b5 )  -gul  -(
+aou  -ain )
* Reg # 7
* WALL; assigned material: Aluminium; mat # (10)
WALL       5 +( +gul  -a )  -rin  -bb  -( +flu1  -flu11 )
* Reg # 8
* A1; assigned material: Aluminium; mat # (10)
A1         5 +a1  -iron
* Reg # 9
* Iron; assigned material: Iron; mat # (11)
Iron       5 +iron
* Reg # 10
* ROOM; assigned material: Oxygen; mat # (8)
ROOM       5 +rin  -targ
* Reg # 11
* targ; assigned material: Tungsten; mat # (23)
targ       5 +targ
* Reg # 12
* AA; assigned material: Gold; mat # (15)
AA         5 +aou  -ain
* Reg # 13
* FLU1; assigned material: Blackhole; mat # (1)
FLU1       5 +flu1  -flu11
* Reg # 14
* FLU3; assigned material: Blackhole; mat # (1)
FLU3       5 +flu3  -flu33
* Reg # 15
* FLU4; assigned material: Blackhole; mat # (1)
FLU4       5 +flu4  -flu3
* Reg # 36
* FLU4; assigned material: Blackhole; mat # (1)
FLU5       5 +flu6  -flu5
* Reg # 16
* B1; assigned material: Blackhole; mat # (1)
B1         5 +b2  -b1
* Reg # 17
* B2; assigned material: Blackhole; mat # (1)
B2         5 +b3  -b2
* Reg # 18
* B3; assigned material: Blackhole; mat # (1)
B3         5 +b4  -b3
* Reg # 19
```

```
* B4; assigned material: Blackhole; mat # (1)
B4          5 +b5  -b4
* Reg # 20
* B5; assigned material: Blackhole; mat # (1)
B5          5 +b6  -b5
* Reg # 21
* A2; assigned material: Blackhole; mat # (1)
A2          5 +a2  -iron
* Reg # 22
* A3; assigned material: Blackhole; mat # (1)
A3          5 +a3  -iron
* Reg # 23
* A4; assigned material: Blackhole; mat # (1)
A4          5 +a4  -iron
* Reg # 24
* A5; assigned material: Blackhole; mat # (1)
A5          5 +a5
* Reg # 25
* A6; assigned material: Blackhole; mat # (1)
A6          5 +a6
* Reg # 26
* A7; assigned material: Blackhole; mat # (1)
A7          5 +a7
* Reg # 27
* C1; assigned material: Gold; mat # (15)
C1          5 +c1
* Reg # 28
* C2; assigned material: Gold; mat # (15)
C2          5 +c2
* Reg # 29
* C3; assigned material: Gold; mat # (15)
C3          5 +c3
* Reg # 30
* C4; assigned material: Gold; mat # (15)
C4          5 +c4
* Reg # 31
* C5; assigned material: Gold; mat # (15)
C5          5 +c5
* Reg # 32
* C6; assigned material: Gold; mat # (15)
C6          5 +c6
* Reg # 33
* C7; assigned material: Gold; mat # (15)
C7          5 +c7
```

```
* Reg # 34
* C8; assigned material: Gold; mat # (15)
C8            5 +c8
* Reg # 35
* C9; assigned material: Gold; mat # (15)
C9            5 +c9
END
GEOEND
ASSIGNMA      BLCKHOLE       BLK
ASSIGNMA           AIR       VOID
ASSIGNMA         CONCR        CON
ASSIGNMA         CONCR        FUL
ASSIGNMA      BLCKHOLE        TV3
ASSIGNMA         CONCR          H
ASSIGNMA         CONCR       WALL
ASSIGNMA         CONCR         A1
ASSIGNMA         CONCR       Iron
ASSIGNMA           AIR       ROOM
ASSIGNMA          LEAD       targ
ASSIGNMA         CONCR         AA
ASSIGNMA         CONCR       FLU1
ASSIGNMA         CONCR       FLU3
ASSIGNMA           AIR       FLU4
ASSIGNMA           AIR       FLU5
ASSIGNMA        CONCRH         B1
ASSIGNMA        CONCRH         B2
ASSIGNMA        CONCRH         B3
ASSIGNMA        CONCRH         B4
ASSIGNMA        CONCRH         B5
ASSIGNMA         CONCR         A2
ASSIGNMA         CONCR         A3
ASSIGNMA         CONCR         A4
ASSIGNMA         CONCR         A5
ASSIGNMA         CONCR         A6
ASSIGNMA         CONCR         A7
ASSIGNMA         CONCR         C1
ASSIGNMA         CONCR         C2
ASSIGNMA         CONCR         C3
ASSIGNMA         CONCR         C4
ASSIGNMA         CONCR         C5
ASSIGNMA         CONCR         C6
ASSIGNMA         CONCR         C7
ASSIGNMA         CONCR         C8
ASSIGNMA         CONCR         C9
```

```
BIASING         0.0         1.0      0.001        ROOM
BIASING         0.0         1.0     0.0027        WALL
BIASING         0.0         1.0     0.0074          B1
BIASING         0.0         1.0     0.0074          A1
BIASING         0.0         1.0     0.0074         TV3
BIASING         0.0         1.0       0.02          B2
BIASING         0.0         1.0     0.0074          A2
BIASING         0.0         1.0      0.054          B3
BIASING         0.0         1.0     0.0074          A3
BIASING         0.0         1.0      0.148          AA
BIASING         0.0         1.0      0.148          B4
BIASING         0.0         1.0     0.0074          A4
BIASING         0.0         1.0      0.403          B5
BIASING         0.0         1.0     0.0074          A5
BIASING         0.0         1.0        1.1         FUL
BIASING         0.0         1.0     0.0074          A6
BIASING         0.0         1.0       2.98         CON
BIASING         0.0         1.0       2.98          A7
BIASING         0.0         1.0     0.0001          C1
BIASING         0.0         1.0     0.0001          C2
BIASING         0.0         1.0     0.0001          C3
BIASING         0.0         1.0     0.0001          C4
BIASING         0.0         1.0     0.0001          C5
BIASING         0.0         1.0     0.0001          C6
BIASING         0.0         1.0     0.0001          C7
BIASING         0.0         1.0     0.0001          C8
BIASING         0.0         1.0     0.0001          C9
MATERIAL                             2.4         26.             CONCR
MATERIAL        19.      39.093     0.862         27.             POTASSIU
MATERIAL        16.      32.066      2.06         28.             SULFUR
MATERIAL         0.          0.   1.29E-3         29.             AIR
COMPOUND       -0.5    HYDROGEN     -10.4      CARBON    -49.3    OXYGENCONCR
COMPOUND       -1.7    MAGNESIU       -.4    ALUMINUM      -.1    IRONCONCR
COMPOUND       -1.5     SILICON      -0.0                       -35.8  CALCIUMCONCR
COMPOUND        -.1    TITANIUM       -.1    POTASSIU      -.3    SULFURCONCR
COMPOUND       -76.    NITROGEN      -24.      OXYGEN             AIR
MATERIAL        24.     51.9961      7.18                         CHROMIUM
MATERIAL        25.   54.938049      7.21                         MANGANES
MATERIAL        15.   30.973761      1.82                         PHOSPHO
MATERIAL        42.       95.94     10.22         33.             MOLYBDEN
MATERIAL        27.     58.9332       8.9                         COBALT
MATERIAL                             4.2                          CONCRH
COMPOUND       0.28    HYDROGEN      0.01      CARBON    32.13    OXYGENCONCRH
COMPOUND        2.1     CALCIUM      0.21    MAGNESIU    63.96    IRONCONCRH
```

```
COMPOUND          0.25   ALUMINUM      0.89   ALUMINUM      0.02     SODIUMCONCRH
COMPOUND          0.05   CALCIUM       0.03   TITANIUM      0.16     ARGONCONCRH
* ambient dose equivalent for all particles
USRBIN           11.     DOSE-EQ      -25.    1000.                 2300.DOSE
USRBIN            0.0                 -100.    200.    200.    200. &
AUXSCORE      USRBIN  ALL-PART                DOSE                     AMB74
* ambient dose equivalent for all particles
USRBIN           12.     DOSE-EQ       38.    FLU4                 @LASTREGDOSE1
USRBIN          FLU4                  -100.     1.    100.    200. &
AUXSCORE      USRBIN  ALL-PART                DOSE1                    AMB74
* ambient dose equivalent for all particles
USRBIN           12.     DOSE-EQ       39.    FLU5                 @LASTREGDOSE2
USRBIN          FLU5                  -100.     1.    100.    200. &
AUXSCORE      USRBIN  ALL-PART                DOSE2                    AMB74
USRTRACK         -1.     NEUTRON      -21.    FLU1   7822566.       260.FL1n
USRTRACK          1.     1E-14                                          &
USRTRACK         -1.     ELECTRON     -22.    FLU1   7822566.       260.FL1e
USRTRACK          1.     1E-04                                          &
USRTRACK         -1.     PROTON       -23.    FLU1   7822566.       260.FL1p
USRTRACK          1.     1E-04                                          &
USRTRACK         -1.     PHOTON       -24.    FLU1   7822566.       260.FL1g
USRTRACK          1.     1E-04                                          &
USRTRACK         -1.     PION+        -40.    FLU1   7822566.       260.FL1pi
USRTRACK          1.     1E-04                                          &
USRTRACK         -1.     NEUTRON      -30.    FLU3  17090264.       260.FL3n
USRTRACK          1.     1E-14                                          &
USRTRACK         -1.     ELECTRON     -31.    FLU3  17090264.       260.FL3e
USRTRACK          1.     1E-04                                          &
USRTRACK         -1.     PROTON       -32.    FLU3  17090264.       260.FL3p
USRTRACK          1.     1E-04                                          &
USRTRACK         -1.     PHOTON       -33.    FLU3  17090264.       260.FL3g
USRTRACK          1.     1E-04                                          &
USRTRACK         -1.     PION+        -41.    FLU3  17090264.       260.FL3pi
USRTRACK          1.     1E-04                                          &
USRTRACK         -1.     NEUTRON      -34.    FLU4  47123890.       260.FL4n
USRTRACK          1.     1E-14                                          &
USRTRACK         -1.     ELECTRON     -35.    FLU4  47123890.       260.FL4e
USRTRACK          1.     1E-04                                          &
USRTRACK         -1.     PROTON       -36.    FLU4  47123890.       260.FL4p
USRTRACK          1.     1E-04                                          &
USRTRACK         -1.     PHOTON       -37.    FLU4  47123890.       260.FL4g
USRTRACK          1.     1E-04                                          &
USRTRACK         -1.     PION+        -42.    FLU4  47123890.       260.FL4pi
USRTRACK          1.     1E-04                                          &
```

```
USRTRACK        -1.    NEUTRON    -43.       FLU5 47123890.    260.FL5n
USRTRACK         1.     1E-14                                         &
USRTRACK        -1.   ELECTRON    -44.       FLU5 47123890.    260.FL5e
USRTRACK         1.     1E-14                                         &
USRTRACK        -1.     PROTON    -45.       FLU5 47123890.    260.FL5p
USRTRACK         1.     1E-14                                         &
USRTRACK        -1.     PHOTON    -46.       FLU5 47123890.    260.FL5g
USRTRACK         1.     1E-14                                         &
USRTRACK        -1.      PION+    -47.       FLU5 47123890.   260.FL5pi
USRTRACK         1.     1E-14                                         &
BEAM           -0.4                          -1.0       -1.0     HEAVYION
HI-PROPE        10.      20.
BEAMPOS          0.       0.     600.
RANDOMIZ         1. 32308439.
START          5E5
STOP
```

6.1.2 Input File: Air Activation

Input file of the air activation simulations for the primary Ne-20.

```
TITLE
Ne20
GLOBAL        1000.0       0.0       0.0       0.0       1.0       0.
DEFAULTS                                                        PRECISIO
GEOBEGIN                                                        COMBNAME
   0   0        MC-CAD
SPH blk        0. 0.00 0.00 2000.00
RPP wall       -430. 430. -30. 520. -30. 1230.
RPP room       -400. 400. 0. 490. 0. 1200.
RCC targ       0. 125. 340. 0. 0. 50. 2.5
END
BLK         5 +blk  -wall
WALL        5 +wall -room
ROOM        5 +room -targ
TARG        5 +targ
END
GEOEND
ASSIGNMA    BLCKHOLE       BLK
ASSIGNMA       CONCR      WALL
ASSIGNMA        Luft      ROOM
ASSIGNMA        LEAD      TARG                          VACUUM
MATERIAL                              2.4      26.                 CONCR
```

6 Appendix

```
MATERIAL          19.       39.093      0.862        27.                          POTASSIU
MATERIAL          16.       32.066       2.06        28.                          SULFUR
MATERIAL           0.           0.     1.29E-3        29.                          Luft
COMPOUND         -0.5    HYDROGEN      -10.4     CARBON      -49.3     OXYGENCONCR
COMPOUND         -1.7    MAGNESIU        -.4   ALUMINUM        -.1     IRONCONCR
COMPOUND         -1.5     SILICON       -0.0                -35.8     CALCIUMCONCR
COMPOUND          -.1    TITANIUM        -.1   POTASSIU        -.3     SULFURCONCR
COMPOUND     -75.5267    NITROGEN   -23.1781     OXYGEN    -1.2827     ARGONLuft
COMPOUND     -0.01248      CARBON                                      Luft
MATERIAL          24.     51.9961       7.18                          CHROMIUM
MATERIAL          25.   54.938049       7.21                          MANGANES
MATERIAL          15.   30.973761       1.82                          PHOSPHO
MATERIAL          42.       95.94      10.22        33.                          MOLYBDEN
MATERIAL          27.     58.9332        8.9                          COBALT
MATERIAL                                 4.2                          CONCRH
COMPOUND         0.28    HYDROGEN       0.01     CARBON      32.13     OXYGENCONCRH
COMPOUND          2.1     CALCIUM       0.21   MAGNESIU      63.96     IRONCONCRH
COMPOUND         0.25    ALUMINUM       0.89   ALUMINUM       0.02     SODIUMCONCRH
COMPOUND         0.05     CALCIUM       0.03   TITANIUM       0.16     ARGONCONCRH
PHYSICS            3.                                                  EVAPORAT
*PHYSICS           1.         0.1                                      1.IONSPLIT
PHYSICS            1.                                                  1.COALESCE
RESNUCLE           3.         22.        31.         50.       ROOM    470.4E6res_target
RESNUCLE           3.        -23.        31.         50.       ROOM    470.4E6res_target
RADDECAY           1.                 3.111111101.  1001000.
USRBIN            10.    ALL-PART       -24.        400.       470.    1200.ROOM
USRBIN          -400.          0.         0.        200.        10.     200. &
USRTRACK          -1.     NEUTRON       -21.        ROOM    470.4E6     200.Fluence
USRTRACK           1.        1E-14                                           &
DCYSCORE           1.                            res_target              RESNUCLE
IRRPROFI      116129.        2E10
DCYTIMES           0.
BEAM             -0.4                                          1.0       1.0     HEAVYION
HI-PROPE          10.         20.
BEAMPOS            0.        125.       300.
RANDOMIZ           1.   12399765.
START             2E6
STOP
```

6.1.3 Output File: Air Activation

Output (sum.lis) file of the air activation simulations for the primary Ne-20.

```
**** Ne20_23.rnc ****


Total primaries run:          8000000


Total weight of the primaries run:    8000000.00



Detector n:              1   res_target
(Region          3  Volume:     470400000.      cmc,
distr. type  :            3     ,
Z_max:          31 , N-Z_max:          45 , N-Z_min:          -4 )

Tot. response (n/cmc/pr)   2.59015409E-09   +/-   9.29837376E-02  %
( --> Nuclei/pr            1.21840847       +/-   9.29837376E-02  % )

**** Isotope Yield as a function of Mass Number **** ****          (nuclei / cmc / pr)



A_min:        1  -  A_max:         107

A:          76  2.6573128E-16 +/-   9.9000000E+01 %
A:          69  2.6573128E-16 +/-   9.9000000E+01 %
A:          67  2.6573128E-16 +/-   9.9000000E+01 %
A:          64  2.6573128E-16 +/-   9.9000000E+01 %
A:          62  2.6573128E-16 +/-   9.9000000E+01 %
A:          59  2.6573128E-16 +/-   9.9000000E+01 %
A:          47  5.3146256E-16 +/-   5.7735027E+01 %
A:          46  2.6573128E-16 +/-   9.9000000E+01 %
A:          42  2.6573128E-16 +/-   9.9000000E+01 %
A:          41  2.1338223E-12 +/-   1.1246643E+00 %
A:          40  2.0450681E-12 +/-   9.7813542E-01 %
A:          39  3.1967474E-13 +/-   3.3810057E+00 %
A:          38  2.1045919E-13 +/-   4.8966470E+00 %
A:          37  1.5864158E-13 +/-   4.1696994E+00 %
A:          36  6.9621598E-14 +/-   6.8984438E+00 %
A:          35  3.5076531E-14 +/-   8.9209713E+00 %
A:          34  3.9593962E-14 +/-   9.6404745E+00 %
A:          33  2.4181547E-14 +/-   6.3127062E+00 %
A:          32  1.4615221E-14 +/-   4.5756575E+00 %
A:          31  1.3552296E-14 +/-   1.4803597E+01 %
A:          30  1.1160714E-14 +/-   8.2478605E+00 %
A:          29  9.5663263E-15 +/-   1.3608276E+01 %
```

6 Appendix

```
A:          28  5.3146259E-15 +/-   8.1649663E+00 %
A:          27  2.6573129E-15 +/-   4.1633319E+01 %
A:          26  3.9859692E-15 +/-   2.2771002E+01 %
A:          25  2.1258503E-15 +/-   2.0412415E+01 %
A:          24  1.3286565E-15 +/-   5.0332231E+01 %
A:          23  2.1258504E-15 +/-   3.5355340E+01 %
A:          22  5.3146256E-16 +/-   5.7735027E+01 %
A:          21  1.8601190E-15 +/-   2.7355060E+01 %
A:          20  5.0488945E-15 +/-   1.7977108E+01 %
A:          19  1.3286564E-15 +/-   3.8297084E+01 %
A:          18  1.4083758E-14 +/-   4.7483250E+00 %
A:          17  8.4502551E-14 +/-   2.6435046E+00 %
A:          16  1.3807398E-11 +/-   4.5881472E-01 %
A:          15  4.6472949E-11 +/-   2.2350823E-01 %
A:          14  1.0960321E-09 +/-   1.0254500E-01 %
A:          13  2.3440423E-11 +/-   2.2123891E-01 %
A:          12  1.9552243E-11 +/-   5.1929632E-01 %
A:          11  7.3385416E-11 +/-   1.4746499E-01 %
A:          10  5.3948768E-12 +/-   9.6647696E-01 %
A:           9  2.3875956E-12 +/-   1.2181594E+00 %
A:           8  5.1844176E-13 +/-   2.4191775E+00 %
A:           7  4.8445471E-12 +/-   1.0274450E+00 %
A:           6  5.2062075E-12 +/-   5.8541022E-01 %
A:           4  1.4884805E-10 +/-   1.6505654E-01 %
A:           3  1.4449671E-11 +/-   4.8186801E-01 %
A:           2  2.6581899E-11 +/-   1.9827702E-01 %
A:           1  1.1040197E-09 +/-   9.0254923E-02 %

**** Isotope Yield as a function of Atomic Number **** ****
  (nuclei / cmc / pr)                     ****


Z_min:         1  -  Z_max:          31

Z:          31  7.9719385E-16 +/-   6.3828474E+01 %
Z:          28  7.9719385E-16 +/-   3.3333333E+01 %
Z:          22  2.6573128E-16 +/-   9.9000000E+01 %
Z:          21  2.6573128E-16 +/-   9.9000000E+01 %
Z:          20  2.6573128E-16 +/-   9.9000000E+01 %
Z:          19  5.3146258E-15 +/-   3.1622776E+01 %
Z:          18  4.7066327E-12 +/-   4.3567259E-01 %
Z:          17  2.0620748E-13 +/-   2.8467425E+00 %
Z:          16  1.0576105E-13 +/-   2.8867145E+00 %
Z:          15  3.4545068E-14 +/-   5.1025000E+00 %
```

```
Z:              14   2.5510204E-14 +/-    1.1023964E+01 %
Z:              13   9.5663263E-15 +/-    1.6355111E+01 %
Z:              12   6.3775508E-15 +/-    2.3570227E+01 %
Z:              11   3.1887755E-15 +/-    2.7216553E+01 %
Z:              10   5.8460883E-15 +/-    1.5745918E+01 %
Z:               9   7.7062074E-15 +/-    2.2786469E+01 %
Z:               8   1.4948979E-11 +/-    3.6679792E-01 %
Z:               7   1.1405081E-10 +/-    1.2055203E-01 %
Z:               6   1.0712649E-09 +/-    9.4790507E-02 %
Z:               5   7.6370642E-11 +/-    1.2737548E-01 %
Z:               4   4.9675808E-12 +/-    1.0573960E+00 %
Z:               3   9.2184841E-12 +/-    5.3733629E-01 %
Z:               2   1.5333333E-10 +/-    1.8812196E-01 %
Z:               1   1.1408804E-09 +/-    9.1969614E-02 %


**** Residual nuclei distribution  **** ****    (nuclei / cmc / pr)         ****



A \ Z  21       22       23       24       25       26       27       28       29       30       31
76   0.00E+00  0.00E+00  0.00E+00  0.00E+00  0.00E+00  0.00E+00  0.00E+00  0.00E+00  0.00E+00  0.00E+00  2.66E-16
 +/- 0.0 %  +/- 0.0 %  +/- 0.0 %  +/- 0.0 %  +/- 0.0 %  +/- 0.0 %  +/- 0.0 %  +/- 0.0 %  +/- 0.0 %  +/- 0.0 %  +/-99.0 %
69   0.00E+00  0.00E+00  0.00E+00  0.00E+00  0.00E+00  0.00E+00  0.00E+00  0.00E+00  0.00E+00  0.00E+00  2.66E-16
 +/- 0.0 %  +/- 0.0 %  +/- 0.0 %  +/- 0.0 %  +/- 0.0 %  +/- 0.0 %  +/- 0.0 %  +/- 0.0 %  +/- 0.0 %  +/- 0.0 %  +/-99.0 %
67   0.00E+00  0.00E+00  0.00E+00  0.00E+00  0.00E+00  0.00E+00  0.00E+00  0.00E+00  0.00E+00  0.00E+00  2.66E-16
 +/- 0.0 %  +/- 0.0 %  +/- 0.0 %  +/- 0.0 %  +/- 0.0 %  +/- 0.0 %  +/- 0.0 %  +/- 0.0 %  +/- 0.0 %  +/- 0.0 %  +/-99.0 %
64   0.00E+00  0.00E+00  0.00E+00  0.00E+00  0.00E+00  0.00E+00  0.00E+00  2.66E-16  0.00E+00  0.00E+00  0.00E+00
 +/- 0.0 %  +/- 0.0 %  +/- 0.0 %  +/- 0.0 %  +/- 0.0 %  +/- 0.0 %  +/- 0.0 %  +/-99.0 %  +/- 0.0 %  +/- 0.0 %  +/- 0.0 %
62   0.00E+00  0.00E+00  0.00E+00  0.00E+00  0.00E+00  0.00E+00  0.00E+00  2.66E-16  0.00E+00  0.00E+00  0.00E+00
 +/- 0.0 %  +/- 0.0 %  +/- 0.0 %  +/- 0.0 %  +/- 0.0 %  +/- 0.0 %  +/- 0.0 %  +/-99.0 %  +/- 0.0 %  +/- 0.0 %  +/- 0.0 %
59   0.00E+00  0.00E+00  0.00E+00  0.00E+00  0.00E+00  0.00E+00  0.00E+00  2.66E-16  0.00E+00  0.00E+00  0.00E+00
 +/- 0.0 %  +/- 0.0 %  +/- 0.0 %  +/- 0.0 %  +/- 0.0 %  +/- 0.0 %  +/- 0.0 %  +/-99.0 %  +/- 0.0 %  +/- 0.0 %  +/- 0.0 %
47   2.66E-16  2.66E-16  0.00E+00  0.00E+00  0.00E+00  0.00E+00  0.00E+00  0.00E+00  0.00E+00  0.00E+00  0.00E+00
 +/-99.0 %  +/-99.0 %  +/- 0.0 %  +/- 0.0 %  +/- 0.0 %  +/- 0.0 %  +/- 0.0 %  +/- 0.0 %  +/- 0.0 %  +/- 0.0 %  +/- 0.0 %

A \ Z  10       11       12       13       14       15       16       17       18       19       20
46   0.00E+00  0.00E+00  0.00E+00  0.00E+00  0.00E+00  0.00E+00  0.00E+00  0.00E+00  0.00E+00  0.00E+00  2.66E-16
 +/- 0.0 %  +/- 0.0 %  +/- 0.0 %  +/- 0.0 %  +/- 0.0 %  +/- 0.0 %  +/- 0.0 %  +/- 0.0 %  +/- 0.0 %  +/- 0.0 %  +/-99.0 %
42   0.00E+00  0.00E+00  0.00E+00  0.00E+00  0.00E+00  0.00E+00  0.00E+00  0.00E+00  2.66E-16  0.00E+00  0.00E+00
 +/- 0.0 %  +/- 0.0 %  +/- 0.0 %  +/- 0.0 %  +/- 0.0 %  +/- 0.0 %  +/- 0.0 %  +/- 0.0 %  +/-99.0 %  +/- 0.0 %  +/- 0.0 %
41   0.00E+00  0.00E+00  0.00E+00  0.00E+00  0.00E+00  0.00E+00  0.00E+00  2.66E-16  2.13E-12  2.66E-16  0.00E+00
 +/- 0.0 %  +/- 0.0 %  +/- 0.0 %  +/- 0.0 %  +/- 0.0 %  +/- 0.0 %  +/- 0.0 %  +/-99.0 %  +/- 1.1 %  +/-99.0 %  +/- 0.0 %
40   0.00E+00  0.00E+00  0.00E+00  0.00E+00  0.00E+00  0.00E+00  0.00E+00  9.83E-15  2.03E-12  2.39E-15  0.00E+00
 +/- 0.0 %  +/- 0.0 %  +/- 0.0 %  +/- 0.0 %  +/- 0.0 %  +/- 0.0 %  +/- 0.0 %  +/- 9.2 %  +/- 1.0 %  +/-45.8 %  +/- 0.0 %
39   0.00E+00  0.00E+00  0.00E+00  0.00E+00  0.00E+00  0.00E+00  0.00E+00  4.73E-14  2.70E-12  2.66E-15  0.00E+00
 +/- 0.0 %  +/- 0.0 %  +/- 0.0 %  +/- 0.0 %  +/- 0.0 %  +/- 0.0 %  +/- 0.0 %  +/-10.6 %  +/- 3.3 %  +/-20.0 %  +/- 0.0 %
38   0.00E+00  0.00E+00  0.00E+00  0.00E+00  0.00E+00  0.00E+00  0.00E+00  1.59E-15  1.57E-14  1.78E-13  0.00E+00  0.00E+00
 +/- 0.0 %  +/- 0.0 %  +/- 0.0 %  +/- 0.0 %  +/- 0.0 %  +/- 0.0 %  +/- 0.0 %  +/-43.0 %  +/- 6.6 %  +/- 4.7 %  +/- 0.0 %  +/- 0.0 %
37   0.00E+00  0.00E+00  0.00E+00  0.00E+00  0.00E+00  0.00E+00  7.17E-15  6.30E-14  8.85E-14  0.00E+00  0.00E+00
 +/- 0.0 %  +/- 0.0 %  +/- 0.0 %  +/- 0.0 %  +/- 0.0 %  +/- 0.0 %  +/-22.9 %  +/- 9.0 %  +/- 5.0 %  +/- 0.0 %  +/- 0.0 %
36   0.00E+00  0.00E+00  0.00E+00  0.00E+00  0.00E+00  0.00E+00  2.52E-14  3.99E-14  4.52E-15  0.00E+00  0.00E+00
 +/- 0.0 %  +/- 0.0 %  +/- 0.0 %  +/- 0.0 %  +/- 0.0 %  +/- 0.0 %  +/- 7.6 %  +/- 7.0 %  +/-11.3 %  +/- 0.0 %  +/- 0.0 %
35   0.00E+00  0.00E+00  0.00E+00  0.00E+00  0.00E+00  1.33E-15  1.99E-14  1.38E-14  0.00E+00  0.00E+00  0.00E+00
 +/- 0.0 %  +/- 0.0 %  +/- 0.0 %  +/- 0.0 %  +/- 0.0 %  +/-50.3 %  +/-10.3 %  +/-20.1 %  +/- 0.0 %  +/- 0.0 %  +/- 0.0 %
34   0.00E+00  0.00E+00  0.00E+00  0.00E+00  0.00E+00  4.78E-15  3.40E-14  3.99E-16  0.00E+00  0.00E+00  0.00E+00
 +/- 0.0 %  +/- 0.0 %  +/- 0.0 %  +/- 0.0 %  +/- 0.0 %  +/-23.1 %  +/-12.3 %  +/-33.3 %  +/- 0.0 %  +/- 0.0 %  +/- 0.0 %
33   0.00E+00  0.00E+00  0.00E+00  0.00E+00  2.66E-16  1.01E-14  1.38E-14  0.00E+00  0.00E+00  0.00E+00  0.00E+00
 +/- 0.0 %  +/- 0.0 %  +/- 0.0 %  +/- 0.0 %  +/-99.0 %  +/- 5.3 %  +/- 9.4 %  +/- 0.0 %  +/- 0.0 %  +/- 0.0 %  +/- 0.0 %
32   0.00E+00  0.00E+00  0.00E+00  0.00E+00  1.86E-15  8.77E-15  3.99E-15  0.00E+00  0.00E+00  0.00E+00  0.00E+00
 +/- 0.0 %  +/- 0.0 %  +/- 0.0 %  +/- 0.0 %  +/-48.8 %  +/-15.9 %  +/-27.5 %  +/- 0.0 %  +/- 0.0 %  +/- 0.0 %  +/- 0.0 %
31   0.00E+00  0.00E+00  0.00E+00  0.00E+00  4.78E-15  8.77E-15  0.00E+00  0.00E+00  0.00E+00  0.00E+00  0.00E+00
 +/- 0.0 %  +/- 0.0 %  +/- 0.0 %  +/- 0.0 %  +/-19.2 %  +/-17.4 %  +/- 0.0 %  +/- 0.0 %  +/- 0.0 %  +/- 0.0 %  +/- 0.0 %
30   0.00E+00  0.00E+00  0.00E+00  7.97E-16  9.57E-15  7.97E-16  0.00E+00  0.00E+00  0.00E+00  0.00E+00  0.00E+00
 +/- 0.0 %  +/- 0.0 %  +/- 0.0 %  +/-63.8 %  +/- 7.9 %  +/-33.3 %  +/- 0.0 %  +/- 0.0 %  +/- 0.0 %  +/- 0.0 %  +/- 0.0 %
29   0.00E+00  0.00E+00  0.00E+00  3.19E-15  6.38E-15  0.00E+00  0.00E+00  0.00E+00  0.00E+00  0.00E+00  0.00E+00
 +/- 0.0 %  +/- 0.0 %  +/- 0.0 %  +/-23.6 %  +/-23.6 %  +/- 0.0 %  +/- 0.0 %  +/- 0.0 %  +/- 0.0 %  +/- 0.0 %  +/- 0.0 %
28   0.00E+00  0.00E+00  0.00E+00  2.66E-15  2.66E-15  0.00E+00  0.00E+00  0.00E+00  0.00E+00  0.00E+00  0.00E+00
 +/- 0.0 %  +/- 0.0 %  +/- 0.0 %  +/-25.8 %  +/-20.0 %  +/- 0.0 %  +/- 0.0 %  +/- 0.0 %  +/- 0.0 %  +/- 0.0 %  +/- 0.0 %
```

```
27  0.00E+00   0.00E+00   2.66E-16   2.39E-15   0.00E+00   0.00E+00   0.00E+00   0.00E+00   0.00E+00   0.00E+00   0.00E+00
   +/- 0.0 %  +/- 0.0 %  +/-99.0 %  +/-38.0 %  +/- 0.0 %  +/- 0.0 %  +/- 0.0 %  +/- 0.0 %  +/- 0.0 %  +/- 0.0 %  +/- 0.0 %
26  0.00E+00   2.66E-16   3.19E-15   2.66E-16   0.00E+00   0.00E+00   0.00E+00   0.00E+00   0.00E+00   0.00E+00   0.00E+00
   +/- 0.0 %  +/-99.0 %  +/-19.2 %  +/-99.0 %  +/- 0.0 %  +/- 0.0 %  +/- 0.0 %  +/- 0.0 %  +/- 0.0 %  +/- 0.0 %  +/- 0.0 %
25  0.00E+00   5.31E-16   1.59E-15   0.00E+00   0.00E+00   0.00E+00   0.00E+00   0.00E+00   0.00E+00   0.00E+00   0.00E+00
   +/- 0.0 %  +/-57.7 %  +/-19.2 %  +/- 0.0 %  +/- 0.0 %  +/- 0.0 %  +/- 0.0 %  +/- 0.0 %  +/- 0.0 %  +/- 0.0 %  +/- 0.0 %
24  0.00E+00   0.00E+00   1.33E-15   0.00E+00   0.00E+00   0.00E+00   0.00E+00   0.00E+00   0.00E+00   0.00E+00   0.00E+00
   +/- 0.0 %  +/- 0.0 %  +/-50.3 %  +/- 0.0 %  +/- 0.0 %  +/- 0.0 %  +/- 0.0 %  +/- 0.0 %  +/- 0.0 %  +/- 0.0 %  +/- 0.0 %
23  0.00E+00   2.13E-15   0.00E+00   0.00E+00   0.00E+00   0.00E+00   0.00E+00   0.00E+00   0.00E+00   0.00E+00   0.00E+00
   +/- 0.0 %  +/-35.4 %  +/- 0.0 %  +/- 0.0 %  +/- 0.0 %  +/- 0.0 %  +/- 0.0 %  +/- 0.0 %  +/- 0.0 %  +/- 0.0 %  +/- 0.0 %
22  2.66E-16   0.00E+00   0.00E+00   0.00E+00   0.00E+00   0.00E+00   0.00E+00   0.00E+00   0.00E+00   0.00E+00   0.00E+00
   +/-99.0 %  +/- 0.0 %  +/- 0.0 %  +/- 0.0 %  +/- 0.0 %  +/- 0.0 %  +/- 0.0 %  +/- 0.0 %  +/- 0.0 %  +/- 0.0 %  +/- 0.0 %
21  1.33E-15   2.66E-16   0.00E+00   0.00E+00   0.00E+00   0.00E+00   0.00E+00   0.00E+00   0.00E+00   0.00E+00   0.00E+00
   +/-20.0 %  +/-99.0 %  +/- 0.0 %  +/- 0.0 %  +/- 0.0 %  +/- 0.0 %  +/- 0.0 %  +/- 0.0 %  +/- 0.0 %  +/- 0.0 %  +/- 0.0 %
20  4.25E-15   0.00E+00   0.00E+00   0.00E+00   0.00E+00   0.00E+00   0.00E+00   0.00E+00   0.00E+00   0.00E+00   0.00E+00
   +/-20.4 %  +/- 0.0 %  +/- 0.0 %  +/- 0.0 %  +/- 0.0 %  +/- 0.0 %  +/- 0.0 %  +/- 0.0 %  +/- 0.0 %  +/- 0.0 %  +/- 0.0 %

A \ Z    1          2          3          4          5          6          7          8          9
22  0.00E+00   0.00E+00   0.00E+00   0.00E+00   0.00E+00   0.00E+00   0.00E+00   0.00E+00   2.66E-16
   +/- 0.0 %  +/- 0.0 %  +/- 0.0 %  +/- 0.0 %  +/- 0.0 %  +/- 0.0 %  +/- 0.0 %  +/- 0.0 %  +/-99.0 %
21  0.00E+00   0.00E+00   0.00E+00   0.00E+00   0.00E+00   0.00E+00   0.00E+00   0.00E+00   2.66E-16
   +/- 0.0 %  +/- 0.0 %  +/- 0.0 %  +/- 0.0 %  +/- 0.0 %  +/- 0.0 %  +/- 0.0 %  +/- 0.0 %  +/-99.0 %
20  0.00E+00   0.00E+00   0.00E+00   0.00E+00   0.00E+00   0.00E+00   0.00E+00   2.66E-16   5.31E-16
   +/- 0.0 %  +/- 0.0 %  +/- 0.0 %  +/- 0.0 %  +/- 0.0 %  +/- 0.0 %  +/- 0.0 %  +/-99.0 %  +/-57.7 %
19  0.00E+00   0.00E+00   0.00E+00   0.00E+00   0.00E+00   0.00E+00   0.00E+00   0.00E+00   1.33E-15
   +/- 0.0 %  +/- 0.0 %  +/- 0.0 %  +/- 0.0 %  +/- 0.0 %  +/- 0.0 %  +/- 0.0 %  +/- 0.0 %  +/-38.3 %
18  0.00E+00   0.00E+00   0.00E+00   0.00E+00   0.00E+00   0.00E+00   0.00E+00   1.09E-14   3.19E-15
   +/- 0.0 %  +/- 0.0 %  +/- 0.0 %  +/- 0.0 %  +/- 0.0 %  +/- 0.0 %  +/- 0.0 %  +/- 8.3 %  +/-13.6 %
17  0.00E+00   0.00E+00   0.00E+00   0.00E+00   0.00E+00   0.00E+00   4.52E-15   7.79E-14   2.13E-15
   +/- 0.0 %  +/- 0.0 %  +/- 0.0 %  +/- 0.0 %  +/- 0.0 %  +/- 0.0 %  +/-11.3 %  +/- 1.8 %  +/-35.4 %
16  0.00E+00   0.00E+00   0.00E+00   0.00E+00   0.00E+00   2.66E-16   4.62E-13   1.33E-11   0.00E+00
   +/- 0.0 %  +/- 0.0 %  +/- 0.0 %  +/- 0.0 %  +/- 0.0 %  +/-99.0 %  +/- 2.4 %  +/- 0.4 %  +/- 0.0 %
15  0.00E+00   0.00E+00   0.00E+00   0.00E+00   0.00E+00   1.09E-14   4.50E-11   1.44E-12   0.00E+00
   +/- 0.0 %  +/- 0.0 %  +/- 0.0 %  +/- 0.0 %  +/- 0.0 %  +/-12.2 %  +/- 0.2 %  +/- 1.3 %  +/- 0.0 %
14  0.00E+00   0.00E+00   0.00E+00   2.66E-16   5.31E-16   1.03E-09   6.57E-11   7.84E-14   0.00E+00
   +/- 0.0 %  +/- 0.0 %  +/- 0.0 %  +/-99.0 %  +/-57.7 %  +/- 0.1 %  +/- 0.3 %  +/- 4.3 %  +/- 0.0 %
13  2.66E-16   0.00E+00   0.00E+00   0.00E+00   7.79E-14   2.05E-11   2.88E-12   1.33E-15   0.00E+00
   +/-99.0 %  +/- 0.0 %  +/- 0.0 %  +/- 0.0 %  +/- 5.6 %  +/- 0.2 %  +/- 1.0 %  +/-20.0 %  +/- 0.0 %
12  0.00E+00   0.00E+00   0.00E+00   0.00E+00   1.33E-15   4.84E-13   1.90E-11   1.81E-14   0.00E+00
   +/- 0.0 %  +/- 0.0 %  +/- 0.0 %  +/-20.0 %  +/- 2.1 %  +/- 0.5 %  +/-18.3 %  +/- 0.0 %  +/- 0.0 %
11  0.00E+00   0.00E+00   2.66E-16   2.18E-14   7.20E-11   1.34E-12   0.00E+00   0.00E+00   0.00E+00
   +/- 0.0 %  +/- 0.0 %  +/-99.0 %  +/-10.6 %  +/- 0.2 %  +/- 1.2 %  +/- 0.0 %  +/- 0.0 %  +/- 0.0 %
10  0.00E+00   0.00E+00   0.00E+00   1.62E-12   3.69E-12   8.58E-14   0.00E+00   0.00E+00   0.00E+00
   +/- 0.0 %  +/- 0.0 %  +/- 0.0 %  +/- 1.9 %  +/- 0.9 %  +/- 5.4 %  +/- 0.0 %  +/- 0.0 %  +/- 0.0 %
 9  0.00E+00   0.00E+00   5.82E-14   2.32E-12   0.00E+00   9.30E-15   0.00E+00   0.00E+00   0.00E+00
   +/- 0.0 %  +/- 0.0 %  +/- 0.5 %  +/- 1.2 %  +/- 0.0 %  +/-18.3 %  +/- 0.0 %  +/- 0.0 %  +/- 0.0 %
 8  0.00E+00   4.25E-15   4.23E-13   0.00E+00   9.17E-14   0.00E+00   0.00E+00   0.00E+00   0.00E+00
   +/- 0.0 %  +/-17.7 %  +/- 2.0 %  +/- 0.0 %  +/- 5.6 %  +/- 0.0 %  +/- 0.0 %  +/- 0.0 %  +/- 0.0 %
 7  0.00E+00   0.00E+00   3.84E-12   1.00E-12   0.00E+00   0.00E+00   0.00E+00   0.00E+00   0.00E+00
   +/- 0.0 %  +/- 0.0 %  +/- 1.1 %  +/- 1.1 %  +/- 0.0 %  +/- 0.0 %  +/- 0.0 %  +/- 0.0 %  +/- 0.0 %
 6  0.00E+00   3.10E-13   4.90E-12   0.00E+00   0.00E+00   0.00E+00   0.00E+00   0.00E+00   0.00E+00
   +/- 0.0 %  +/- 1.3 %  +/- 0.7 %  +/- 0.0 %  +/- 0.0 %  +/- 0.0 %  +/- 0.0 %  +/- 0.0 %  +/- 0.0 %
 4  0.00E+00   1.49E-10   0.00E+00   0.00E+00   0.00E+00   0.00E+00   0.00E+00   0.00E+00   0.00E+00
   +/- 0.0 %  +/- 0.2 %  +/- 0.0 %  +/- 0.0 %  +/- 0.0 %  +/- 0.0 %  +/- 0.0 %  +/- 0.0 %  +/- 0.0 %
 3  1.03E-11   4.17E-12   0.00E+00   0.00E+00   0.00E+00   0.00E+00   0.00E+00   0.00E+00   0.00E+00
   +/- 0.4 %  +/- 1.3 %  +/- 0.0 %  +/- 0.0 %  +/- 0.0 %  +/- 0.0 %  +/- 0.0 %  +/- 0.0 %  +/- 0.0 %
 2  2.66E-11   0.00E+00   0.00E+00   0.00E+00   0.00E+00   0.00E+00   0.00E+00   0.00E+00   0.00E+00
   +/- 0.2 %  +/- 0.0 %  +/- 0.0 %  +/- 0.0 %  +/- 0.0 %  +/- 0.0 %  +/- 0.0 %  +/- 0.0 %  +/- 0.0 %
 1  1.10E-09   0.00E+00   0.00E+00   0.00E+00   0.00E+00   0.00E+00   0.00E+00   0.00E+00   0.00E+00
   +/- 0.1 %  +/- 0.0 %  +/- 0.0 %  +/- 0.0 %  +/- 0.0 %  +/- 0.0 %  +/- 0.0 %  +/- 0.0 %  +/- 0.0 %
```

```
**** Isomers (nuclei / cmc / pr)      ****
A        Z        mth
26       13       1      2.66E-16 +/- 99.0 %
34       17       1      3.99E-16 +/- 33.3 %
38       17       1      1.57E-14 +/-  6.6 %
```

6.2 Raw Data of Dose Simulations Outside the Shielding

In this section the raw data of ambient dose equivalent simulations outside the shielding of IR1 and IR3 are listed.

6.2.1 Ambient Dose Equivalent Rates per Primary Particle for IR1

Nuclide	"far" [pSv/primary]	"close" [pSv/primary]	"far" uncertainty [pSv/primary]	"close" uncertainty [pSv/primary]
p250	0.000073	0.000071	0.000023	0.000017
H2	0.001606	0.001425	0.000447	0.000661
He3	0.002384	0.001561	0.001049	0.000363
He4	0.002648	0.001995	0.000182	0.000428
Li6	0.005611	0.003071	0.000926	0.000588
Li7	0.006785	0.004475	0.001406	0.000750
Be9	0.007745	0.005720	0.001242	0.001029
B10	0.008934	0.006307	0.001170	0.001150
B11	0.010191	0.007098	0.001259	0.000989
C12	0.010496	0.007137	0.002837	0.001780
C13	0.011144	0.008933	0.000243	0.001105
N14	0.012042	0.009336	0.001684	0.000407
N15	0.016243	0.008662	0.001074	0.000927
O16	0.012937	0.009829	0.000798	0.000947
O17	0.015166	0.010256	0.002175	0.000775
O18	0.017692	0.012082	0.001186	0.001388
F19	0.018075	0.011461	0.002320	0.001036
Ne20	0.017830	0.012311	0.001743	0.001075
Ne21	0.019336	0.011797	0.001744	0.000839
Ne22	0.020672	0.014704	0.001358	0.001505

6.2.2 Ambient Dose Equivalent Rates per primary particle for IR3

Nuclide	"far" [pSv/primary]	"close" [pSv/primary]	"far" uncertainty [pSv/primary]	"close" uncertainty [pSv/primary]
1H	1.0903E-01	8.1466E-02	2.2799E-03	2.7946E-03
2H	4.1519E-01	4.0699E-01	4.2135E-03	8.4855E-03
3He	2.5624E-01	2.3942E-01	7.8282E-03	7.1515E-03
4He	4.2950E-01	4.0894E-01	1.8324E-02	8.2470E-03
6Li	5.7286E-01	5.3298E-01	9.1626E-03	2.5208E-02
7Li	8.2323E-01	7.9321E-01	2.2601E-02	2.5201E-02
9Be	8.1480E-01	8.1853E-01	6.3455E-02	1.5841E-02
10B	6.8595E-01	6.1853E-01	2.9173E-02	2.2437E-02
11B	8.3677E-01	7.7168E-01	1.6143E-02	1.8723E-02
12C	6.6317E-01	6.5737E-01	1.5854E-02	2.5093E-02
13C	8.1498E-01	8.0054E-01	1.2155E-02	2.8584E-02
14N	7.1470E-01	6.7732E-01	2.1997E-02	2.0448E-02
15N	8.3277E-01	7.9477E-01	2.4212E-02	2.8279E-02
16O	7.5025E-01	7.1062E-01	4.9219E-02	4.9264E-02
17O	8.4851E-01	8.0427E-01	3.6798E-03	1.8969E-02
18O	9.5667E-01	9.5418E-01	3.5628E-02	4.4169E-02
19F	8.6955E-01	8.4587E-01	3.3828E-02	2.0929E-02
20Ne	7.7273E-01	7.5398E-01	2.8791E-02	3.2029E-02
21Ne	8.6222E-01	8.6733E-01	1.3947E-02	2.3703E-02
22Ne	9.9338E-01	9.5364E-01	1.6390E-02	3.1687E-02

6.3 Additional Data Concerning the Activation of Air

In this section additional data concerning the activation of air is shown in several bar charts. First, the comparison of the activity of activation products for the remaining primary particles to the authorized p800. Second, the absolute activity values of the activation products.
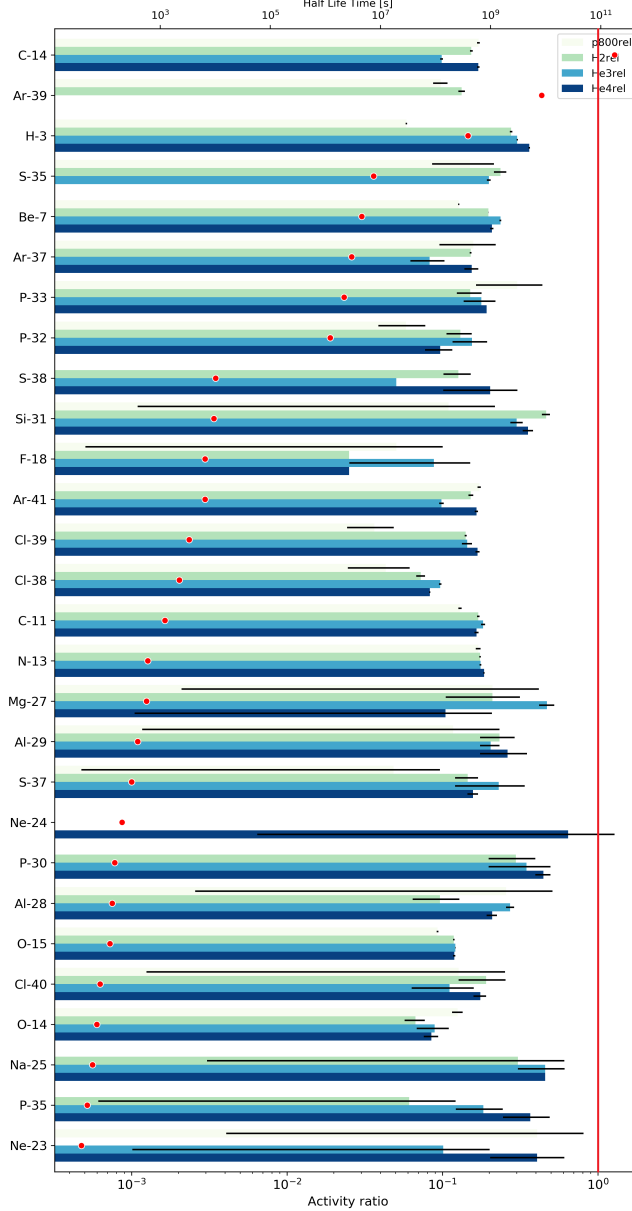
Figure 6.1: Activation products from primaries p800 (newly simulated with $2E9$ *primaries/s*) to He-4 (in various colors) are shown on the y-axis. The ratio to the authorized p800 from the work of Karacson[3] is shown on the bottom x-axis. The values are sorted by their half life time, which is also plotted on the top x-axis together with red points. The red line indicates where the ratio of activities is one.
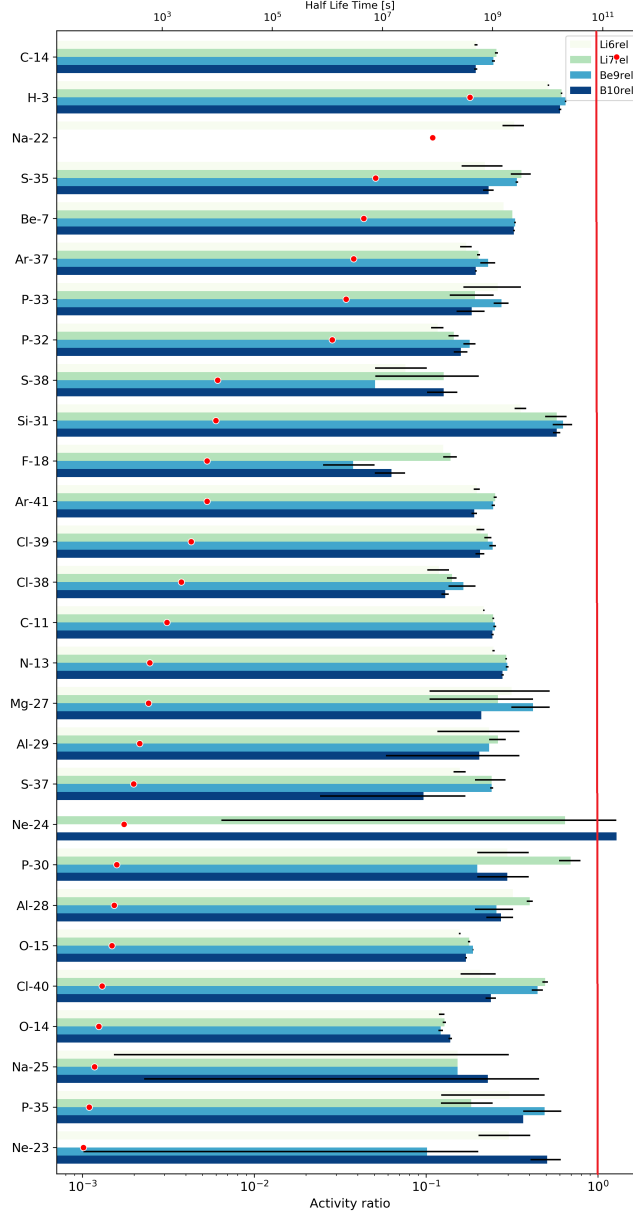
Figure 6.2: Activation products from primaries Li-6 to B-10 (in various colors) are shown on the y-axis. The ratio to the authorized p800 from the work of Karacson[3] is shown on the bottom x-axis. The values are sorted by their half life time, which is also plotted on the top x-axis together with red points. The red line indicates where the ratio of activities is one.
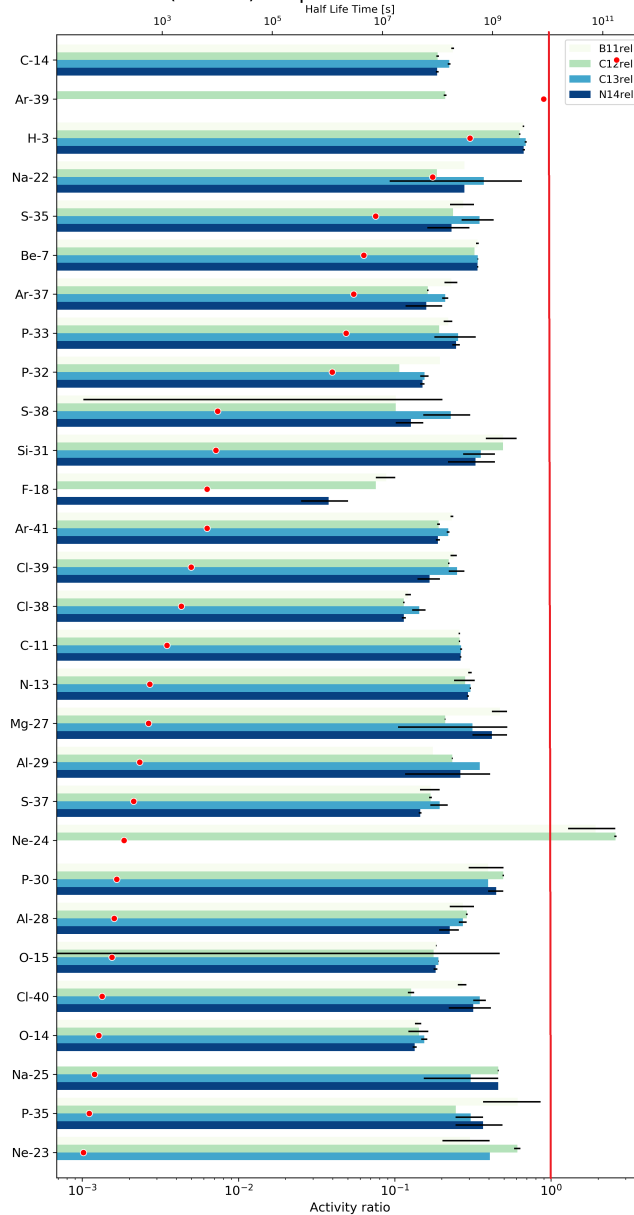
Figure 6.3: Activation products from primaries B-11 to N-14 (in various colors) are shown on the y-axis. The ratio to the authorized p800 from the work of Karacson[3] is shown on the bottom x-axis. The values are sorted by their half life time, which is also plotted on the top x-axis together with red points. The red line indicates where the ratio of activities is one.
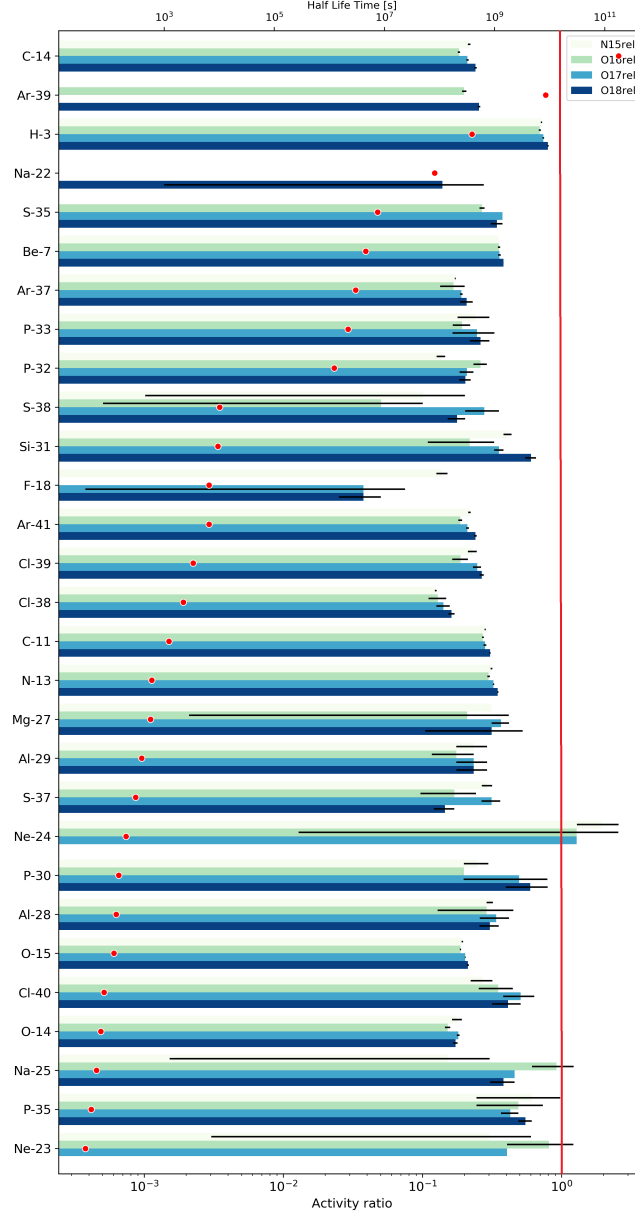
Figure 6.4: Activation products from primaries N-15 to O-18 (in various colors) are shown on the y-axis. The ratio to the authorized p800 from the work of Karacson[3] is shown on the bottom x-axis. The values are sorted by their half life time, which is also plotted on the top x-axis together with red points. The red line indicates where the ratio of activities is one.
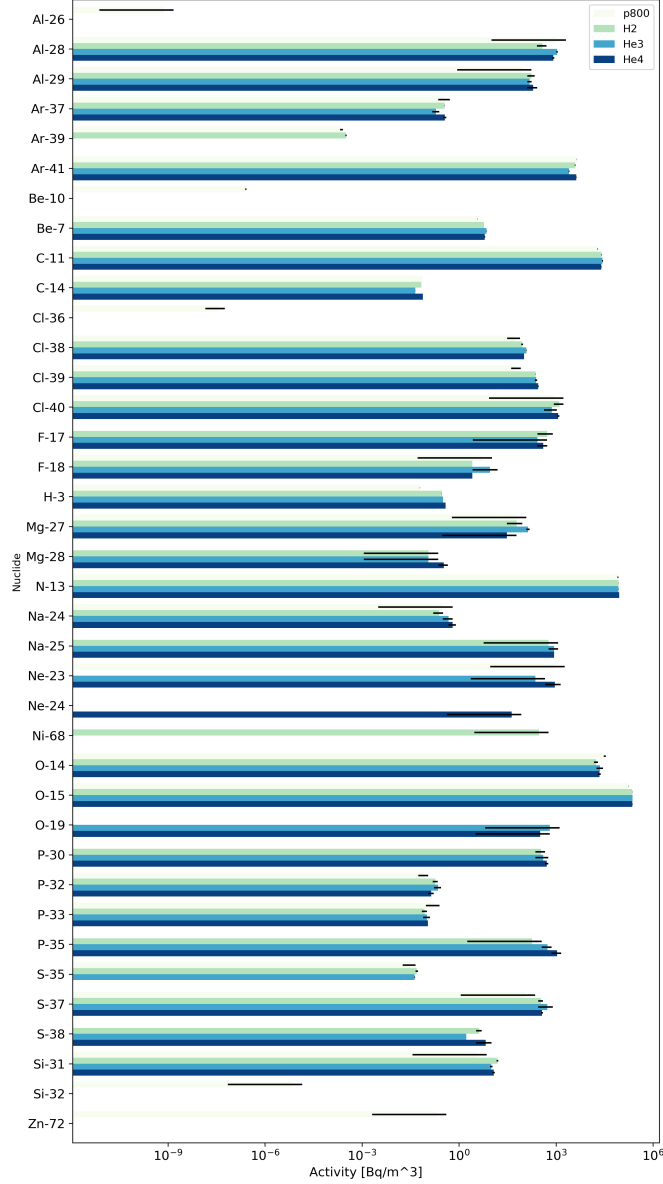
Figure 6.5: Activation products from primaries p800 (newly simulated with
2*E*9 *primaries/s*) to He-4 (in various colors) are shown on the y-axis. The
corresponding absolute activities are plotted on the x-axis.
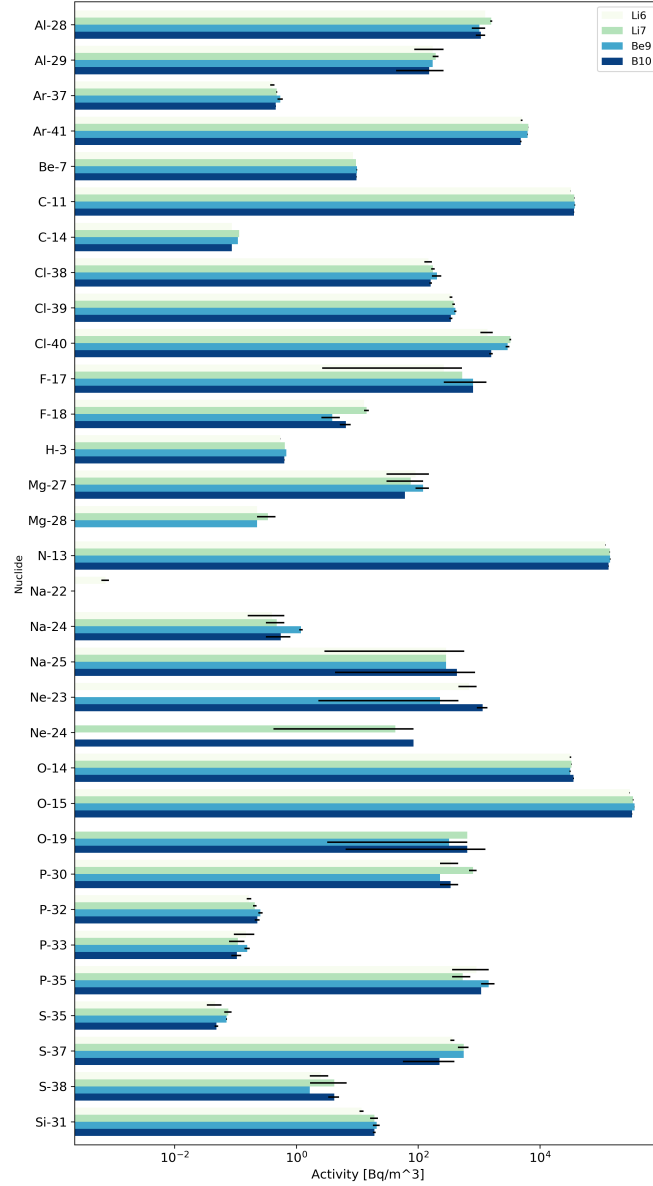
Figure 6.6: Activation products from primaries Li-6 to B-10 (in various colors) are shown on the y-axis. The corresponding absolute activities are plotted on the x-axis.
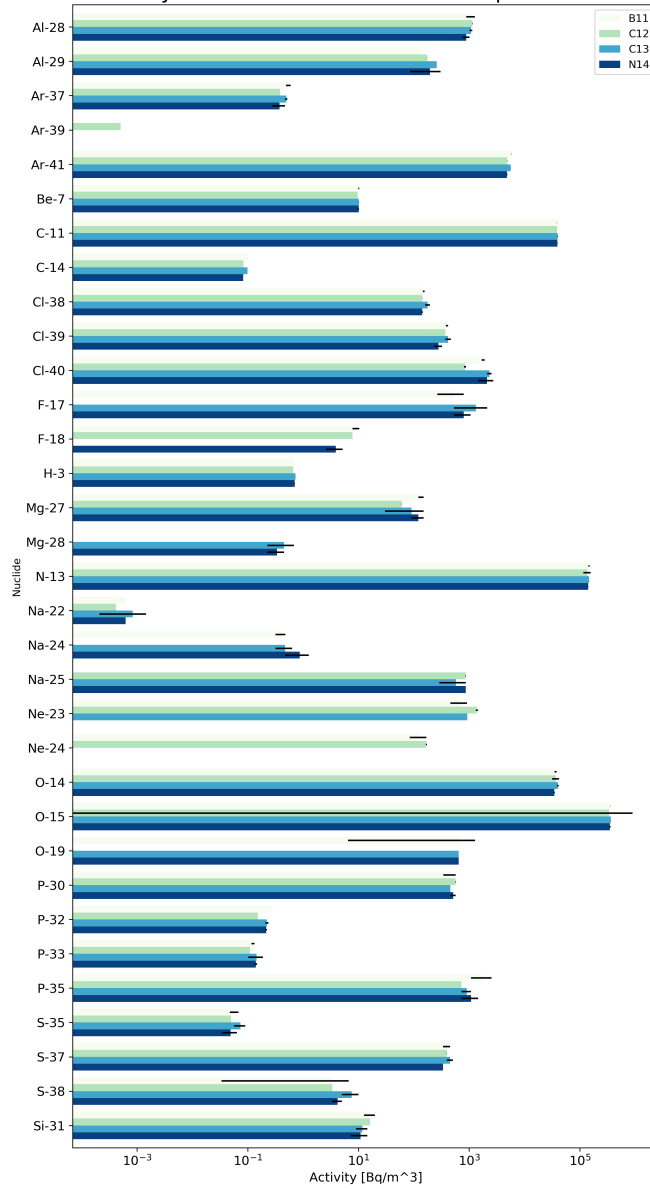
Figure 6.7: Activation products from primaries B-11 to N-14 (in various colors) are shown on the y-axis. The corresponding absolute activities are plotted on the x-axis.
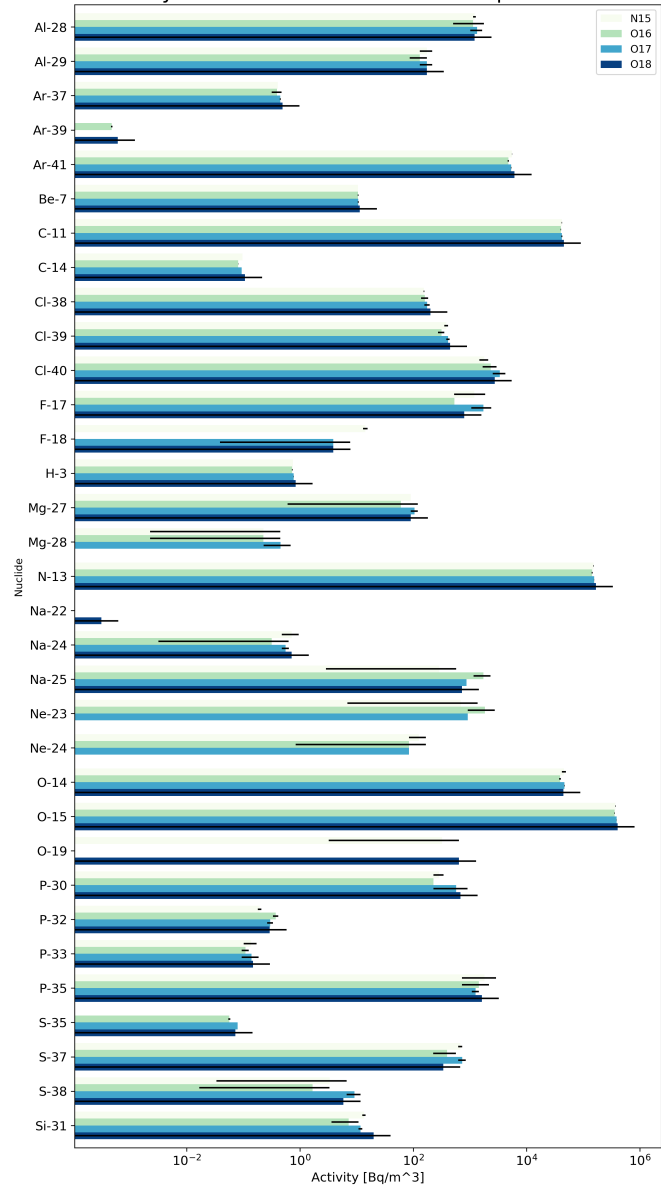
Figure 6.8: Activation products from primaries N-15 to O-18 (in various colors) are shown on the y-axis. The corresponding absolute activities are plotted on the x-axis.
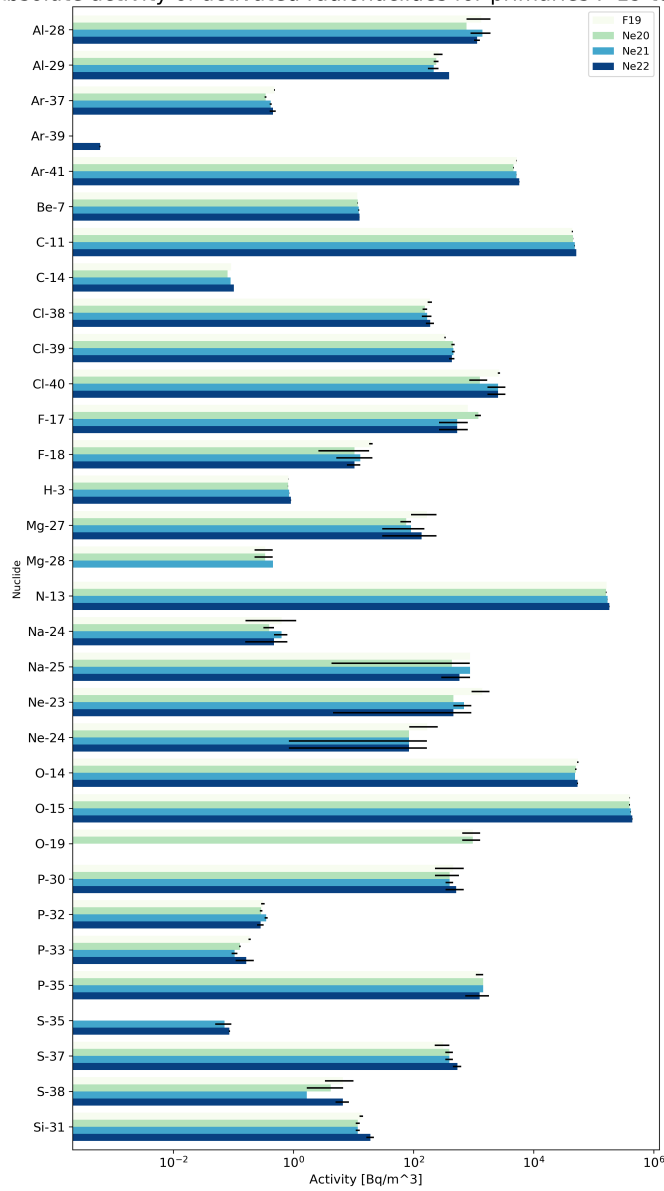
Figure 6.9: Activation products from primaries F-19 to Ne-22 (in various colors) are shown on the y-axis. The corresponding absolute activities are plotted on the x-axis.

Bibliography

[1] Jägerhofer, Lukas. Shielding and Radiation studies for MedAustron. Wien. (2011)

[2] Feldbaumer, Eduard. Strahlenphysikalische Untersuchung einer Spziellen Schicht-bauweise als Innovative Abschirmung für Hochenergie-Ionenbeschleuniger. Graz. (2013)

[3] Matthias, Karacson. Monte Carlo simulation of the activation of air at the MedAustron project. Wien. (2010)

[4] EBG MedAustron GmbH

[5] A.M. Sessler. Introduction to Ion Beam Cancer Therapy. Lawrence Berkeley National Laboratory. Berkeley. (2010)

[6] R.R. Wilson. Radiological Use of Fast Protons. 47, 487. (1946)

[7] U. Amaldi. History of Hadron Therapy. Modern Physics Letters. (2005)

[8] Bragg Curves and Peaks. Brookhaven National Laboratory. (2016)

[9] A. Walker. Radiobiology Basics. Training Course on Radiation Dosimetry. University of Ontario Institute of Technology. (2012)

[10] St James, S., Grassberger, C., and Lu, H. M.; Considerations when treating lung cancer with passive scatter or active scanning proton therapy. Translational lung cancer research, 7(2), 210–215. (2018)

[11] Bourhaleb, Faiza, Attili, Andrea and Russo, Germano. Monte Carlo Simulations for Beam Delivery Line Design in Radiation Therapy with Heavy Ion Beams. 10.5772/15883. (2011)

[12] D. Georg, Motivation for Ions Species Beyond Protons and Carbon Ions, (2020)

[13] Anas M. El-Mahdi et al.; A Comparison of Radiation Control of Pulmonary Metastases in C3H Mice by Helium Ions or Cobald-60 Photons. Cancer 34. 130-135. (1974)

[14] John T. Lyman et al.; A Helium Ion Beam for Stereoatactic Radiosurgery of Central Nervous System Disorders, Donner Laboratory and Donner Pavilion. University of California. Berkeley. (1986)

64

[15] Grün, R., Friedrich, T., Krämer, M., Zink, K., Durante, M., Engenhart-Cabillic, R. and Scholz, M.; Assessment of potential advantages of relevant ions for particle therapy: A model based study. Med. Phys., 42: 1037-1047. (2015)

[16] B. Knäusl, H. Fuchs, K. Dieckmann, D. Georg. Can particle beam therapy be improved using helium ions? – A planning study focusing on pediatric patients. 55. 751-759. (2016)

[17] O. Sokol ,E. Scifoni,M. Kraemer. Oxygen beams for therapy: Advanced biological treatment planning and experimental verification. Physics in Medicine and Biology. 62. (2017)

[18] ICRP Publication 74. Conversion Coefficients for use in Radiological Protection Against External Radiation. (1996)

[19] ICRP Publication 103. The 2007 Recommendations of the International Commission on Radiological Protection. (2007)

[20] A. Alhussain, A. Abuhoza, Comparison Study of Reflected and Transmitted Thermal Neutron Flux in Water and Other Moderators. (2020)

[21] P.M. Rinard. Neutron Interactions with Matter, Passive Nondestructive Assay of Nuclear Material. Los Alamos Technical Report NUREG/CR-5550. LA-UR-90-732; pp. 357-377. (1991)

[22] G. Battistoni, S. Muraro, P.R. Sala, F. Cerutti, A. Ferrari, S. Roesler, A. Fasso', J. Ranft. The FLUKA code: Description and benchmarking , Proceedings of the Hadronic Shower Simulation Workshop 2006. Fermilab 6–8 September 2006. M. Albrow, R. Raja eds.; AIP Conference Proceeding 896; pp. 31-49. (2007)

[23] http://www.fluka.org, 08.05.2020

[24] A.Fasso J. Ranft A. Ferrari, P.R. Sala. Fluka: a multi particle transport code. s.l.: CERN 2005-10. (2005)

[25] C. Theis, K.H. Buchegger, M. Brugger, D. Forkel-Wirth, S. Roesler, H. Vincke, Interactive three dimensional visualization and creation of geometries for Monte Carlo calculations, Nuclear Instruments and Methods in Physics Research A 562, pp. 827-829. (2006)

[26] A. Ferrari, P.R. Sala. Physics of Showers induced by accelerator beams. CEA. "Frederic Joliot" Summer School in Reactor Physics. (1995)

[27] Bertini, Hugo W. Low-Energy Intranuclear Cascade Calculation. Physical Review. Bd. 131, 4 S. 1801-1821. (1963)

[28] Metropolis, N et al. Monte Carlo Calculations on Intranuclear Cascades. I. Low-Energy Studies. Physical Review. Bd. 110, 1, S. 185-203. (1958)

[29] Metropolis, N et al. Monte Carlo Calculations on Intranuclear Cascades. II. High-Energy Studies. Physical Review. Bd. 110, 1, S. 204-219. (1958)

Bibliography

[30] T. Kurosawa et al. Neutron yields from thick C, Al, Cu, and Pb targets bombarded by 400 MeV'nucleon Ar, Fe, Xeand 800 MeV'nucleon Si ions. Japan. (2000)

[31] IAEA Tecdoc. Regulatory Control of the Safety of Ion Radiotherapy Facilities. Vienna. (2020)

[32] Bureau international des poids et mesures. BIPM. Monographie 5. Serves. (2004)

List of Figures

List of Figures

68

List of Tables

Michael Bauer

Curriculum Vitae

Personal Details

Adress	Hausberg 11
	4204 Reichenau, Austria
Mobile	+43 677 616 114 10
E-Mail	michi.bauer@hotmail.com
Born	10.01.1995, Linz, Austria

Work Experience

03/2020–present	**MedAustron**, *Wiener Neustadt*, Intern, Radiation Protection.
	Validation of MedAustron's Shielding Concept for Ions $Z \leq 10$
01/2019–02/2019	**AGES**, *Austrian Agency for Health and Food Safety*, Vienna, Project Work.
	Method Establishment of Gross Alpha and Gross Beta in Water using LSC according to EN ISO 11704
11/2014–09/2015	**Volkshilfe**, *Linz*, Community Service, Disability Care Work.
07/2013–08/2013	**Voestalpine**, *Linz*, Summer Intern, Continous Casting Line.
07/2011–08/2011	**Voestalpine**, *Linz*, Summer Intern, Granulation.

Education

2018–2020	**Technical University of Vienna**, *Biomedical Engineering*, Medical Physics and Imaging, Master's Degree.
2015–2018	**Johannes Kepler University Linz**, *Technical Physics*, Bachelor's Degree.
2013–2014	**Professional Educational Institute**, *Matura*, Linz, Mechanical Engineering.
2009–2013	**School for higher Technical Education**, *Linz*, Mechanical Engineering.

Language and Skills

English, C, Python, FLUKA, CHARMM (MC package for Biomolecules)